NASA TECHNICAL NOTE

NASA TN D-5418

NASA TN D-5418

PRESSURES AND HEAT TRANSFER ON A 75° SWEPT DELTA WING WITH TRAILING-EDGE FLAP AT MACH 6 AND ANGLES OF ATTACK TO 90°

by J. Wayne Keyes

Langley Research Center

Langley Station, Hampton, Va.

NATIONAL AERONAUTICS AND SPACE ADMINISTRATION • WASHINGTON, D. C. • SEPTEMBER 1969

1. Report No. NASA TN D-5418	2. Government Accession No.	3. Recipient's Catalog No.
4. Title and Subtitle PRESSURES AND HEAT TRANSFER ON A 75° SWEPT DELTA WING WITH TRAILING-EDGE FLAP AT MACH 6 AND ANGLES OF ATTACK TO 90°		5. Report Date September 1969 6. Performing Organization Code
7. Author(s) J. Wayne Keyes		8. Performing Organization Report No. L-6096
9. Performing Organization Name and Address NASA Langley Research Center Hampton, Va. 23365		10. Work Unit No. 126-13-10-19-23 11. Contract or Grant No.
12. Sponsoring Agency Name and Address National Aeronautics and Space Administration Washington, D.C. 20546		13. Type of Report and Period Covered Technical Note 14. Sponsoring Agency Code
15. Supplementary Notes		

16. Abstract

An investigation has been made of the effects of deflecting a flap on the flow field on a 75° swept delta wing with sealed gap for angles of attack from 0° to 90°. Pressure and heat-transfer measurements were made with the free-stream Reynolds number (based on wing root chord) varying from 1.3×10^6 to 5.6×10^6 for 0° angle of attack and at 3.4×10^6 for angles greater than 0°. Flap deflections from 0° to 40° were investigated. In general, center-line calculations based on existing two-dimensional methods were in good agreement with the trends of the pressure and heat-transfer distributions if the flow pattern characteristic of the angle-of-attack range and the type of boundary layer are taken into account.

17. Key Words Suggested by Author(s) Delta wing Flap Heat transfer Pressure distributions Shock interaction	18. Distribution Statement Unclassified – Unlimited		
19. Security Classif. (of this report) Unclassified	20. Security Classif. (of this page) Unclassified	21. No. of Pages 44	22. Price* $3.00

*For sale by the Clearinghouse for Federal Scientific and Technical Information
Springfield, Virginia 22151

Page Intentionally Left Blank

PRESSURES AND HEAT TRANSFER ON A 75° SWEPT DELTA WING WITH TRAILING-EDGE FLAP AT MACH 6 AND ANGLES OF ATTACK TO 90°

By J. Wayne Keyes
Langley Research Center

SUMMARY

An investigation has been made of the effect of flap deflection (with sealed gap) on the flow over a delta wing for an angle-of-attack range from 0° to 90° and flap deflections from 0° to 40°. The free-stream Reynolds number (based on the wing root chord) varied from 1.3×10^6 to 5.6×10^6 for 0° angle of attack and was 3.4×10^6 for angles greater than 0°.

Although the flow on the model was found to be complex, a meaningful analysis of the data can be made if the local flow is classified according to the type of boundary layer and according to whether the local Mach number on the wing or flap is less than or greater than 1. Turbulent separation occurred on the wing and flap at approximately 28° flap deflection at 0° angle of attack for a free-stream Reynolds number of 3.4×10^6. This separation trend is consistent with previous two-dimensional studies under similar flow conditions. The strong reflected shock emanating from the intersection of the bow shock and flap shock had a pronounced effect on the pressures and heating in the moderate angle-of-attack range.

In general, even though the flow on the model was three dimensional in nature, center-line calculations based on existing two-dimensional methods were in good agreement with the trends of the pressures and heat transfer except when influenced by the interaction of bow shock and flap shock. Tangent-cone theory and oblique-shock theory predicted the pressure level on the wing and the maximum pressure on the flap, respectively, in the moderate angle-of-attack range. Turbulent heating on the wing was approximated by the modified Spalding-Chi method. Turbulent peak heating on the flap was reasonably well predicted by using a modified Spalding-Chi calculation with the assumption of the virtual origin of turbulent flow at the hinge line and the appropriate inviscid pressure. Estimations of the laminar heating on the wing were made by using the stream-divergence theory in the moderate angle-of-attack range and cross-flow theory in the high angle range.

INTRODUCTION

The design of many hypersonic vehicles requires a knowledge of heat transfer and pressures associated with deflected flaps for either attached or separated flow; of particular interest is the peak heating on deflected flap surfaces and in the separation region. Previous studies of the pressure distribution and heat transfer on both two-dimensional configurations with ramps and delta wings with flaps for attached and separated flows are listed in an extensive bibliography in reference 1. Additional investigations covering delta wings with and without flaps are discussed in references 2, 3, and 4. Most of these studies, however, are primarily for laminar and transitional flows, and only a limited amount of information is available for turbulent flow on delta wings. Vehicles such as a hypersonic cruise configuration will probably be operating with a predominantly turbulent boundary layer over their flaps. The present study, therefore, was initiated to investigate the pressures and heat transfer on a delta wing with trailing-edge flap under turbulent conditions at an angle of attack of 0° with flap deflections up to 40° and for Reynolds numbers up to 27.6×10^{6} per meter. The configuration was also tested at angles of attack up to 90° to investigate the pressures and heat transfer that a reentry or hypersonic glider configuration might encounter while operating at high angle of attack.

The results of this investigation are compared with existing two-dimensional methods of prediction to determine the validity of using these methods for three-dimensional configurations.

SYMBOLS

b_f	flap span, m
$C_{p,p}$	peak pressure coefficient (turbulent) or plateau pressure coefficient (laminar)
c_f	local skin-friction coefficient
c_p	specific heat of air at constant pressure, J/kg-$^{\circ}$K
c_r	delta-wing root chord, m
c_w	specific heat of wall material, J/kg-$^{\circ}$K
h	local heat-transfer coefficient, W/m^2-$^{\circ}$K

L combined length of wing and flap when $\delta = 0^{o}$, m

M_{∞} free-stream Mach number

M_{l} local Mach number

N_{Pr} Prandtl number

$N_{St,\infty}$ local Stanton number based on free-stream conditions ahead of model

p_{∞} free-stream static pressure, N/m^2

p_{l} local wall pressure, N/m^2

$p_{t,\infty}$ free-stream total pressure, N/m^2

q experimental heating rate, W/m^2

R_{∞} free-stream Reynolds number based on delta-wing root chord, $\frac{\rho_{\infty} u_{\infty} c_r}{\mu_{\infty}}$

$R_{\infty,L}$ free-stream Reynolds number based on total length of wing and flap, $\frac{\rho_{\infty} u_{\infty} L}{\mu_{\infty}}$

$R_{\infty,T}$ free-stream Reynolds number based on distance from apex of wing to the end of transition on center line, $\frac{\rho_{\infty} u_{\infty} x_T}{\mu_{\infty}}$

$R_{\infty,v}$ free-stream Reynolds number based on distance from end of transition (virtual origin of turbulent flow) to the hinge line, $\frac{\rho_{\infty} u_{\infty} (x_{HL} - x_T)}{\mu_{\infty}}$

$R_{\infty,x}$ free-stream Reynolds number based on distance along center line of model from apex of wing, $\frac{\rho_{\infty} u_{\infty} x}{\mu_{\infty}}$

R_{l} local Reynolds number based on delta-wing root chord and conditions at outer edge of boundary layer, $\frac{\rho_{l} u_{l} c_r}{\mu_{l}}$

s surface distance from hinge line (positive along flap), m

T_{l} static temperature at outer edge of boundary layer, ^{o}K

T_r	recovery temperature, ^oK
T_w	wall temperature, ^oK
t_w	local measured wall thickness, m
u_∞	free-stream velocity, m/sec
u_l	velocity at outer edge of boundary layer, m/sec
x	distance along center line of model from apex of wing, m
x_{HL}	distance from apex of wing to hinge line, m
x_T	distance from apex of wing to end of transition on center line of model, m
y	spanwise coordinate, m
z_{BL}	calculated boundary-layer thickness at oil accumulation line, m
α	angle of attack of wing center line (positive values indicate compression on instrumented surface), deg
γ	ratio of specific heats of air
Δs	distance from hinge line to oil accumulation line, m
δ	flap deflection angle, deg
η_r	recovery factor
μ_∞	free-stream viscosity, N-sec/m^2
μ_l	viscosity at outer edge of boundary layer, N-sec/m^2
ρ_∞	free-stream density of air, kg/m^3
ρ_l	density of air at outer edge of boundary layer, kg/m^3

ρ_w density of wall material, kg/m^3

τ time, sec

APPARATUS, MODELS, AND TESTS

Tunnel and Model-Injection System

The Langley 20-inch Mach 6 tunnel is a blowdown type exhausting either into the atmosphere or into a vacuum sphere. For these tests it operated at total pressures from about 7.7 to 34 atmospheres and a total temperature of 530° K. A more complete description of the tunnel is given in reference 5.

The model injection system consists of a movable carriage driven by a pneumatic cylinder. A support strut and sting capable of varying the angle of attack are attached to the injector carriage, which is flush with the tunnel wall when the model is in the injected position.

Models

Sketches of the delta wing and flap, showing the location of the pressure orifices and thermocouples, are presented in figure 1. The delta wing had a leading-edge sweep of 75° and the cross section of the leading edge was a sharp 15° double wedge. The flap, which had a planform area equal to 30 percent of the wing planform area, was attached to the wing trailing edge by brackets. A rubber seal was used between the wing and flap to prevent any flow from bleeding through the gap.

Two models were constructed from 405 stainless steel for this investigation. The pressure model was drilled for 0.102-cm inside-diameter tubing, which was increased to 0.178-cm inside diameter to reduce lag effects.

Instrumentation on the heat-transfer model consisted of 30-gage iron-constantan thermocouples. These thermocouples were spotwelded onto the inside surface of slots 1.270 cm wide which were machined deep enough on the upper surface of the heat-transfer model to provide an instrumented skin thickness of approximately 0.076 cm.

For some tests at $\alpha = 30°$ to $\alpha = 60°$, spherical roughness elements were spot-welded to the wing surface of both models for the purpose of tripping the boundary layer. The size, location, and spacing of these elements are shown in figure 1(a).

Tests

The tests were conducted over an angle-of-attack range from 0° to 90° with free-stream Reynolds numbers (based on the wing root chord) of 1.3, 3.4, and 5.6×10^6 for

$\alpha = 0^{\circ}$ and 3.4×10^6 for angles of attack greater than 0°. The trailing-edge flap was deflected in 10° increments up to 40° at the low angles of attack ($\alpha = 0^{\circ}$ and 10°) and up to 30° for $\alpha = 20^{\circ}$ to 60°. The flap remained undeflected ($\delta = 0^{\circ}$) for α greater than 60°. A total temperature of approximately 530° K was used and the average ratio of wall to total temperature was about 0.58.

TEST METHODS AND DATA REDUCTION

Pressure Tests

Pressure distributions were obtained by connecting an individual electrical pressure transducer to each orifice. The output from these transducers was recorded on a digital readout recorder.

Heat-Transfer Tests

The aerodynamic heating was determined by using the thin-skin calorimetric technique to measure the rate of heat storage in the model skin. The model, at approximately room temperature, was suddenly exposed to the airflow by quick injection from a shielded position outside the tunnel. Injection was accomplished in less than 0.25 second and the model remained in the tunnel approximately 4 seconds. The electrical output from the thermocouples was recorded on a high-speed digital readout recorder. The reading from each thermocouple was recorded at 0.05-second intervals, converted to a binary digital system, and recorded on magnetic tape.

Optical and Visual Methods

Schlieren photographs were taken to aid in determining the extent of separation and some aspects of the flow along the wing and flap. In order to examine the surface flow and the boundaries of separation on the wing and flap, the oil-flow technique was employed. A mixture of silicone oil and lampblack was distributed over the model surface in random dots of various sizes. The model was injected and the surface flow streamlines were indicated on the model by oil streaks. The model was then retracted and photographed.

Data Reduction

The heat-transfer data were reduced to Stanton numbers by methods similar to those described in reference 6. Local heating was calculated from the thin-skin equation:

$$q = c_w \rho_w t_w \frac{dT_w}{d\tau}$$

where the time derivative of temperature $dT_w/d\tau$ was obtained from a second-degree curve fitted to the temperature-time data by the method of least squares. Expressions for the specific heats are, for the wing,

$$c_w = 464 + 0.62\left(T_w - 273\right)$$

and for the flap,

$$c_w = 462 + 0.77\left(T_w - 273\right)$$

where T_w is between 273^o and 373^o K. These specific-heat equations were obtained from data measured on an automatic continuous specific-heat tester which had an accuracy of ±2 percent.

The local heat-transfer coefficient was then calculated from the relation

$$h = \frac{q}{T_r - T_w}$$

where T_w is the measured wall temperature and T_r is the calculated recovery temperature defined as

$$T_r = T_l\left(1 + M_l^2 \eta_r \frac{\gamma - 1}{2}\right)$$

The local Mach number outside the boundary layer M_l is calculated from the measured pressure distribution. The total-pressure loss on the wing was obtained from the measured shock angle of the wing for all angles of attack up to the angle of attack where the flow goes subsonic over the complete model ($\alpha = 55^o$). Beyond this angle of attack a normal-shock loss for $M_\infty = 6$ was assumed. A total-pressure loss through the flap shock was calculated from oblique-shock theory and the Mach number on the wing based on measured pressures. When the flap deflection angle exceeded the maximum turning angle for the wing Mach number, a normal-shock loss for that Mach number was assumed (that is, for $\alpha = 40^o$ when $\delta = 30^o$ and for $\alpha = 50^o$ when $\delta = 10^o$, 20^o, and 30^o). All the data were reduced with the assumption that no separation occurred on the wing and flap. These methods were considered adequate since the experimental Stanton number $N_{St,\infty}$ is rather insensitive to small errors in Mach number. In computing the recovery temperature T_r, a recovery factor based on the average N_{Pr} for the complete angle-of-attack range was assumed. The recovery factor was equal to 0.837 for the laminar region and 0.889 for the turbulent region. The Stanton number was calculated from the equation

$$N_{St,\infty} = \frac{h}{\rho_\infty u_\infty c_{p,\infty}}$$

Conduction effects were considered to be negligible, and therefore no correction for conduction has been applied to the data.

RESULTS AND DISCUSSION

Flow Characteristics

If a meaningful analysis of the pressures and heat transfer on a configuration is to be made, the type of boundary layer and local flow field must be considered. In order to determine the type of boundary layer on the model it is necessary to determine where transition occurs.

Transition.- Since the location of boundary-layer transition in wind-tunnel tests is affected by many factors, the position of transition was determined experimentally. The point of maximum heating on the wing and undeflected flap was chosen as the end of transition. These experimental results, which include the effect of free-stream Reynolds number on transition at $\alpha = 0^{\circ}$ and the location of transition at various angles of attack for a given free-stream Reynolds number, are shown in figures 2(a) and 2(b). The calculated local Reynolds number for various angles of attack, based on the local Mach number obtained from experimental pressure data, is shown in figure 2(c).

Transition moves completely off the body between $\alpha = 30^{\circ}$ and $\alpha = 40^{\circ}$ and returns between $\alpha \approx 45^{\circ}$ and $\alpha = 50^{\circ}$. The reason for this reversal is not known, though it should be noted that it occurs near the onset of subsonic flow ($\alpha \approx 55^{\circ}$). It is believed that the boundary layer is turbulent over most of the instrumented surface at $\alpha = 60^{\circ}$ but rapidly becomes laminar over the complete wing and flap at higher angles of attack. A similar trend was noted in reference 7, where it was observed that the boundary layer changed from turbulent to laminar between $\alpha = 60^{\circ}$ and $\alpha = 70^{\circ}$.

Spherical roughness elements located as shown in figure 1(a) were used as boundary-layer trips at angles of attack from 30° to 60°. Figure 2(b) shows that at angles up to 50°, transition occurs much farther forward with roughness than without it. Reference 8 points out that flow distortions may be encountered when using roughness elements to produce turbulent flow on delta wings. Roughness elements were used in the present investigation primarily to confirm the existence of laminar flow at angles of attack around 40° and turbulent flow at 60°. The location and size of the elements used were within the guidelines suggested in reference 8. The heat transfer with and without roughness will be presented later in this paper.

Local flow field.- The local flow in the area of the hinge line is affected by the angle of attack, flap deflection angle, intersection of wing bow shock and flap shock (at moderate angles of attack), and type of boundary layer. The local flow can be classified into the

following flow regimes, which are similar to those of reference 9: (1) supersonic (or hypersonic) on the wing and flap, (2) supersonic on the wing and subsonic on the flap, and (3) subsonic on both wing and flap. Typical measured pressure distributions and schlieren photographs for the various flow regimes are shown in figure 3. Figures 3(a) and 3(e) are examples of supersonic (or hypersonic) and subsonic flow, respectively, over the complete model. Figures 3(b) to 3(d) are included to illustrate that the flow can be very difficult to classify since the flow field is complicated considerably by the intersection of bow shock and flap shock and by separation. These phenomena will be discussed in a subsequent section.

Experimental Results

Low angles of attack ($\alpha < 30^{\circ}$).- Center-line pressures, heat transfer, surface oil-flow patterns, and typical schlieren photographs for zero angle of attack are presented in figures 4, 5, 6, and 7, respectively. The boundary layer on the center line in the vicinity of the hinge line for $\alpha = 0^{\circ}$ is turbulent except for the lowest Reynolds number $\left(R_{\infty} \approx 1.3 \times 10^{6}\right)$ where the boundary layer is transitional (as shown in fig. 2(a)). An inspection of the data shows that the local flow can be classified as hypersonic on the wing and supersonic on the flap. (See fig. 3(a).)

When turbulent flow exists ahead of the hinge line near the center line of the wing, separation occurs at a flap deflection angle of approximately 28° for $\alpha = 0^{\circ}$, as indicated by the results of figure 6. The method used for determining when separation occurs involves taking photographs of the model surface oil-flow patterns at various flap deflection angles, as shown in figure 6(a). The distance from the oil accumulation line to the hinge line Δs is nondimensionalized by the calculated boundary-layer thickness at the oil accumulation line and then plotted as a function of δ. The distance Δs always increases as the flap angle is increased, apparently because any increase in flap pressure is felt upstream through the subsonic portion of the boundary layer. An increase in Δs does not necessarily indicate separation. The assumption was made for this investigation that a rapid increase in Δs signaled the start of separation, as indicated in figure 6(b). (Note that this point occurs where Δs is approximately equal to the calculated boundary-layer thickness.)

It is interesting to note that separation occurred on the delta wing at approximately the same angle as on the flat plates of reference 10 at similar local Mach numbers and Reynolds numbers. This similarity might be expected since the surface oil-flow patterns of figure 6(a) indicate that the attached flow on the delta wing is approximately two-dimensional (oil streaks parallel to the wing center line).

As the flap deflection is increased there is an increase in the separation region, as shown in figure 6. The separation region for $\delta = 40^{\circ}$ contains considerable outward

spanwise flow which forms what appear to be areas of circulatory motion near the shoulder of the leading edge of the wing. (See fig. 6(a).) A similar type of vortex flow was also noted in reference 11. The spanwise differences in the shear forces due to the fact that the boundary layer is turbulent near the center line and laminar near the wing edge, as discussed in reference 11, may contribute to this spanwise flow phenomenon.

Transitional separation occurs at the lowest Reynolds number (1.3×10^6) for all flap deflections at $\alpha = 0^o$, as indicated by the data of figures 4(b) to 4(e). A schlieren photograph for $\delta = 30^o$ is shown in figure 8. Also in this figure is a surface oil-flow photograph which shows that the flow reattached on the flap in a very irregular pattern. The reattaching flow probably is affected by shedding vortex sheets originating along the shoulder of the wing leading edge, and the inward spanwise flow on the flap edges near the wing-flap junction could be due to wing tip effects. Flow similar to this has also been observed in reference 11.

The spanwise variations of pressure and heat transfer at the low angles of attack (0^o and 10^o) are presented in figures 9 and 10, respectively, for $R_\infty \approx 3.4 \times 10^6$. In general, the spanwise pressures at a given chordwise station are nearly constant, except possibly near the edges of the flap and when the flow separates. The end of transition (as indicated by the peaks in the heat-transfer data at various spanwise stations for $\alpha = 0^o$ and $\delta = 0^o$) fell along a line approximately parallel to the leading edge as illustrated by the sketch in figure 10(a).

The trends of the pressures and heat-transfer data at $\alpha = 10^o$ (figs. 9(b) and 10(b)) were similar to those for $\alpha = 0^o$ with the exception of $\delta = 40^o$. At $\alpha = 10^o$ transition has moved farther forward, resulting in a greater turbulent-flow region ahead of separation on the wing. The separation region does not contain the areas of circulatory motion observed at $\alpha = 0^o$ since the flow is predominantly turbulent across the span.

Moderate and high angles of attack ($\alpha \geqq 30^o$).- Pressures and heat transfer are presented in figures 11 and 12, respectively, for the moderate angle-of-attack range ($30^o \leqq \alpha < 60^o$). Some center-line data are included for the wing with spherical roughness elements added to produce turbulent flow. Figure 13 presents typical schlieren photographs. The pressures and heat transfer at the high angles of attack ($\alpha \geqq 60^o$) are shown in figures 14 and 15, respectively.

The local flow field in the area of the flap hinge line for the moderate angle-of-attack range is complicated considerably by the intersection of bow shock and flap shock. When this shock intersection occurs in the proximity of the flap a strong reflected shock is formed, as indicated in the photographs of figure 16(a) for $\alpha = 30^o$ and $\delta = 20^o$. There is a rapid increase in the surface pressures and heating immediately behind the strong reflected shock. It has been shown in reference 9 that when the reflected shock

impinges near the trailing edge of the flap an abrupt change in the flap hinge moment can also result, causing dangerous flap-operation problems.

At an angle of attack of 40° the flow field is extremely complex with a deflected flap. For example, at $\delta = 20^{\circ}$ transitional separation exists and the strong reflected shock impinges near the region of flow reattachment. (See fig. 16(b).) The center-line pressure data indicate that subsonic flow exists on the flap behind the reflected shock (decreasing pressures). Separation was also present on the wing and flap for $\delta = 30^{\circ}$ when $\alpha = 30^{\circ}$ and 40°, as indicated by the pressure data of figures 11(a) and 11(b) and the schlieren photographs of figures 13(a) and 13(b).

As the angle of attack increased further the flap shock and reflected shock were replaced by a strong shock which moved along the wing surface (fig. 13(c)). A region of transonic flow composed of a series of "shock wavelets" was formed behind the strong shock. A shock system similar to this was observed in reference 12 on a delta wing-flap configuration. In the present investigation this shock system disappeared at $\alpha \approx 55^{\circ}$ when the flow became subsonic over the whole configuration.

For the 30° flap deflection the heat-transfer data on the aft part of the wing and flap without roughness, as presented in figure 12, nearly coincides with the roughness data. This similarity might be expected because of the close agreement of the pressure distributions with and without roughness, as shown in figure 11.

The pressures obtained on the wing and flap at the high angles of attack (fig. 14) show the expected trends for subsonic flow in that deflecting the flap did not appreciably change the pressure distribution (except near the flap hinge line for $\alpha = 60^{\circ}$).

An indication that the boundary layer is turbulent over most of the model at $\alpha = 60^{\circ}$ can be seen more clearly in figure 15(a) at $\delta = 0^{\circ}$, where the heat-transfer data with and without roughness is very similar. The rearward movement of transition is indicated in figures 15(b) and 15(c).

Analytical Calculations

In general, two-dimensional methods can be used to obtain good predictions of the levels of the local pressures and heat transfer on the model center line.

Pressure calculations.- The pressures on the wing for attached flow at $\alpha = 0^{\circ}$ were approximately equal to the free-stream static pressure. (See, for example, figs. 3(a), 4, and 9(a).) For angles of attack greater than 0°, tangent-cone theory gave a good prediction of the pressure level on the wing, as indicated in figures 3, 9(b), and 11. Once the flow became subsonic, pressures on the wing were approximated by either the static pressure or the total pressure behind a normal shock at a Mach number of 6, as shown in figure 14.

Pressure calculations on the flap center line for attached flow were obtained by using oblique-shock theory in conjunction with the calculated flow properties on the wing. Good agreement existed between the maximum measured pressures and the calculated pressure levels as long as the flow was not influenced by the interaction of bow shock and flap shock. (See, for example, figs. 4, 9, and 11.)

The separation pressure values presented in figures 4, 9, and 11 were calculated by using the appropriate method for turbulent or laminar separation. The peak pressures for turbulent separation for angles of attack up to 30° were slightly underpredicted by the following empirical equation (eq. (2) of ref. 5):

$$C_{p,p} = 0.13 - \frac{1.5}{M_l^2} + \frac{9.1}{M_l^3}$$

This equation (fitted to experimental data obtained by using forward-facing steps and presented in ref. 5) assumes that Reynolds number has negligible effect on the turbulent peak pressure. The equation is valid when the local Mach numbers ahead of separation are from approximately 3.4 to 6.5. Another empirical equation,

$$C_{p,p} = \frac{3.2}{8 + \left(M_l - 1\right)^2}$$

(eq. (6) of ref. 13) was useful in predicting the peak pressure level at the moderate angle of attack (fig. 11) for lower local Mach numbers ahead of separation. Calculated values of the laminar plateau pressure are included in figure 4 for comparison with the pressures measured in the regions of transitional separation at $R_\infty \approx 1.3 \times 10^6$. These values were calculated from an equation which was originally presented in reference 14 (eq. (17)) and modified in equation (1) of reference 15 as follows:

$$C_{p,p} = \frac{\left(2.61 M_l^{-1/4}\right)\left(c_f\right)^{1/2}}{\left(M_l^2 - 1\right)^{1/4}}$$

The values of the laminar local skin-friction coefficient were determined by the Monaghan T' method of references 16 and 17.

When separation occurred on the wing and flap, values of the maximum pressure on the flap were calculated with the assumption that the flow passed through two shocks. These shocks are caused by an equivalent separation wedge dictated by the pressure rise in the separation region (calculated from the above equations for $C_{p,p}$) and from the resulting angle necessary to turn the flow parallel to the flap. In general, the maximum measured pressure on the flap fell between the values calculated by this method and by the method assuming one shock.

Whenever subsonic flow occurred behind the strong reflected shock on the flap (or behind the bow shock above $\alpha \approx 55^{\circ}$), the local pressure was assumed to decrease parabolically from the location of the shock to the trailing edge. This method, which is discussed more fully in reference 9, gives a fair indication of the trend of the measured pressure, as shown in figures 3(b) to 3(e).

Heat-transfer calculations.- Center-line heating data for the wing and undeflected flap over the complete angle-of-attack range are compared with calculated values in figure 17. The parameter $\left(R_{\infty,x}\right)^{1/2}$ was used to correlate the heat-transfer data. This parameter is based on the free-stream Reynolds number and the diatance from the apex of the wing to a given point on the center line. The heat transfer at the low angles of attack ($\alpha < 30^{\circ}$) falls slightly below the band for turbulent flow calculated by the Spalding-Chi method of reference 18 as modified to heat transfer in reference 19. The limits of the calculated band were taken as the virtual origin of turbulent flow and the flap trailing edge. In the moderate angle-of-attack range, the data are slightly above the values calculated by the laminar stream-divergence method. This method, developed in reference 20 and modified in reference 21, considers the divergence of the surface streamlines. Beyond $\alpha = 60^{\circ}$ the laminar cross-flow theory of reference 22 was used. It is evident from figure 17 that a reasonable prediction of the center-line heating can be obtained by using a method appropriate to the flow pattern peculiar to the angle-of-attack range and also the type of boundary layer present. The cross-flow theory is not really applicable at $\alpha = 80^{\circ}$ and 90° because of the three-dimensional flow, but is included for comparison.

In general, a good indication of the turbulent peak heating level on the flap can be obtained by using the modified Spalding-Chi method except when the flow is influenced by the interaction of bow shock and flap shock. In using this method the virtual origin for the flap boundary layer is assumed to be located at the hinge line as in references 6, 23, and 24. Even though this method does not account for previous growth of the boundary layer, two-dimensional experiments reported in the references have shown that it predicts peak values reasonably well. When the flow is attached, a single-flap-shock loss is assumed which gives a good prediction of the peak heating and the trend of the data (for example, see figs. 5(c), 10, and 12(a)). However, when flow separation occurs, the single-shock loss underpredicts the data. A better prediction of the peak heating (see fig. 5(e)) is obtained when the pressure is calculated on the assumption that the flow passes through two oblique shocks, as discussed in reference 24.

Peak heating in the turbulent separation regions of figures 5 and 10 for $\delta = 40^{\circ}$ was approximated by a method described in reference 6. This method assumes that the local Stanton number remains constant across the separation point.

CONCLUSIONS

An experimental investigation has been made of the effect of flap deflections from 0° to 40° on the pressure and heat-transfer distributions on a 75° swept delta wing with sealed gap at Mach 6 for an angle-of-attack range from 0° to 90°. The free-stream Reynolds number (based on the wing root chord) varied from 1.3×10^6 to 5.6×10^6 for an angle of attack of 0° and was approximately 3.4×10^6 for angles of attack greater than 0°. The ratio of wall to total temperature was 0.58. Conclusions based on the results of this investigation are as follows:

1. A meaningful analysis of the pressures and heat transfer for the complete angle-of-attack range can be made if the local flow is classified according to the type of boundary layer (laminar, transitional, or turbulent) and according to whether the local Mach number on the wing or flap is less than or greater than 1.

2. As the angle of attack increases from 0°, transition moves forward, and then it reverses direction around 10° and moves off the model at higher angles (for a free-stream Reynolds number of 3.4×10^6). At still higher angles of attack, transition returns on the model (around 50°), and it again moves off the model above 60°.

3. When the boundary layer was turbulent near the flap hinge line (free-stream Reynolds number about 3.4×10^6) and supersonic flow was present on the flap, separation did not occur until the flap was deflected to about 28° at 0° angle of attack. This trend is consistent with previous studies of two-dimensional models tested under similar flow conditions.

4. The separation region for a deflection angle of 40° at 0° angle of attack contains considerable outward spanwise flow which form vortices near the leading-edge shoulder. This phenomenon is partially due to the difference in the type of boundary layer across the span for a free-stream Reynolds number of about 5.6×10^6.

5. The local flow field in the area of the flap hinge line for the moderate angle-of-attack range is complicated considerably by the intersection of bow shock and flap shock. The strong reflected shock from this intersection impinges on the wing and flap, causing pronounced changes in the pressure distributions and heat transfer.

6. In general, even though the flow on the wing and flap is three dimensional in nature, center-line calculations based on existing two-dimensional methods were in good agreement with the trends and in some cases predicted the maximum levels of the local pressures and heat transfer. This was not true, however, when the flow was influenced by the interaction of bow shock and flap shock. For example, tangent-cone theory and oblique-shock theory predicted the pressure level on the wing and flap, respectively, in the moderate angle-of-attack range. The modified Spalding-Chi method for turbulent flow was useful in predicting the trend of the heating on the wing. Approximate turbulent peak

heating levels on the flap were calculated by the modified Spalding-Chi method with the virtual origin of turbulent flow assumed to be at the hinge line. Laminar heating on the wing was slightly underpredicted by the stream divergence theory in the moderate angle-of-attack range and cross-flow theory in the high angle range.

Langley Research Center,
National Aeronautics and Space Administration,
Langley Station, Hampton, Va., June 24, 1969,
126-13-10-19-23.

REFERENCES

1. Kaufman, Louis G., II; Meckler, Lawrence H.; Hartofilis, Stavros A.; and Weiss, Daniel: An Investigation of Hypersonic Flow Separation and Control Characteristics. AFFDL-TR-64-174, U.S. Air Force, Jan. 1965.

2. Nagel, A. L.; Fitzsimmons, H. D.; and Doyle, L. B.: Analysis of Hypersonic Pressure and Heat Transfer Tests on Delta Wings With Laminar and Turbulent Boundary Layers. NASA CR-535, 1966.

3. Giles, H. L.; and Thomas, J. W.: Analysis of Hypersonic Pressure and Heat Transfer Tests on a Flat Plate With a Flap and a Delta Wing With Body, Elevons, Fins, and Rudders. NASA CR-536, 1966.

4. Murray, William M., Jr.; and Stallings, Robert L., Jr.: Heat-Transfer and Pressure Distributions on 60° and 70° Swept Delta Wings Having Turbulent Boundary Layers. NASA TN D-3644, 1966.

5. Sterrett, James R.; and Emery, James C.: Extension of Boundary-Layer-Separation Criteria to a Mach Number of 6.5 by Utilizing Flat Plates With Forward-Facing Steps. NASA TN D-618, 1960.

6. Holloway, Paul F.; Sterrett, James R.; and Creekmore, Helen S.: An Investigation of Heat Transfer Within Regions of Separated Flow at a Mach Number of 6.0. NASA TN D-3074, 1965.

7. Paulsen, James J.; and Schadt, Gail H.: A Study of the Pressure and Heat Transfer Distribution on Highly Swept Slab Delta Wings in Supersonic Flow. AIAA Paper No. 66-130, Jan. 1966.

8. Sterrett, James R.; Morrisette, E. Leon; Whitehead, Allen H., Jr.; and Hicks, Raymond M.: Transition Fixing for Hypersonic Flow. NASA TN D-4129, 1967.

9. Keyes, J. Wayne; and Ashby, George C., Jr.: Calculated and Experimental Hinge Moments on a Trailing-Edge Flap of a 75° Swept Delta Wing at Mach 6. NASA TN D-4268, 1967.

10. Sterrett, James R.; and Emery, James C.: Experimental Separation Studies for Two-Dimensional Wedges and Curved Surfaces at Mach Numbers of 4.8 to 6.2. NASA TN D-1014, 1962.

11. Whitehead, Allen H., Jr.; and Keyes, J. Wayne: Flow Phenomena and Separation Over Delta Wings With Trailing-Edge Flaps at Mach 6. AIAA J., vol. 6, no. 12, Dec. 1968, pp. 2380-2387.

12. Fetterman, David E.; and Neal, Luther, Jr.: An Analysis of the Delta-Wing Hypersonic Stability and Control Behavior at Angles of Attack Between 30° and 90°. NASA TN D-1602, 1963.

13. Love, Eugene S.: Pressure Rise Associated With Shock-Induced Boundary-Layer Separation. NACA TN 3601, 1955.

14. Chapman, Dean R.; Kuehn, Donald M.; and Larson, Howard K.: Investigation of Separated Flows in Supersonic and Subsonic Streams With Emphasis on the Effect of Transition. NACA Rep. 1356, 1958. (Supersedes NACA TN 3869.)

15. Sterrett, J. R.; and Holloway, P. F.: On the Effect of Transition on Parameters Within a Separation Region at Hypersonic Speeds – With Emphasis on Heat Transfer. Symposium on Fully Separated Flows, Arthur G. Hansen, ed., Am. Soc. Mech. Engrs., May 1964, pp. 15-26.

16. Monaghan, R. J.: An Approximate Solution of the Compressible Laminar Boundary Layer on a Flat Plate. R. & M. No. 2760, Brit. A.R.C., 1953.

17. Bertram, Mitchel H.; and Feller, William V.: A Simple Method for Determining Heat Transfer, Skin Friction, and Boundary-Layer Thickness for Hypersonic Laminar Boundary-Layer Flows in a Pressure Gradient. NASA MEMO 5-24-59L, 1959.

18. Spalding, D. B.; and Chi, S. W.: The Drag of a Compressible Turbulent Boundary Layer on a Smooth Flat Plate With and Without Heat Transfer. J. Fluid Mech., vol. 18, pt. 1, Jan. 1964, pp. 117-143.

19. Neal, Luther, Jr.; and Bertram, Mitchel H.: Turbulent-Skin-Friction and Heat-Transfer Charts Adapted From the Spalding and Chi Method. NASA TN D-3969, 1967.

20. Vaglio-Laurin, Roberto: Laminar Heat Transfer on Blunt-Nosed Bodies in Three-Dimensional Hypersonic Flow. WADC Tech. Note 58-147, DDC No. AD 155 588, U.S. Air Force, May 1958.

21. Dunavant, James C.: Investigation of Heat Transfer and Pressures on Highly Swept Flat and Dihedral Delta Wings at Mach Numbers of 6.8 and 9.6 and Angles of Attack to 90°. NASA TM X-688, 1962.

22. Bertram, Mitchel H.; and Everhart, Philip E.: An Experimental Study of the Pressure and Heat-Transfer Distribution on a 70° Sweep Slab Delta Wing in Hypersonic Flow. NASA TR R-153, 1963.

23. Becker, John V.; and Korycinski, Peter F.: Heat Transfer and Pressure Distribution at a Mach Number of 6.8 on Bodies With Conical Flares and Extensive Flow Separation. NASA TN D-1260, 1962.

24. Keyes, J. Wayne; Goldberg, Theodore J.; and Emery, James C.: Turbulent Heat Transfer Associated With Control Surfaces at Mach 6. AIAA J., vol. 6, no. 8, Aug. 1968, pp. 1612-1613.

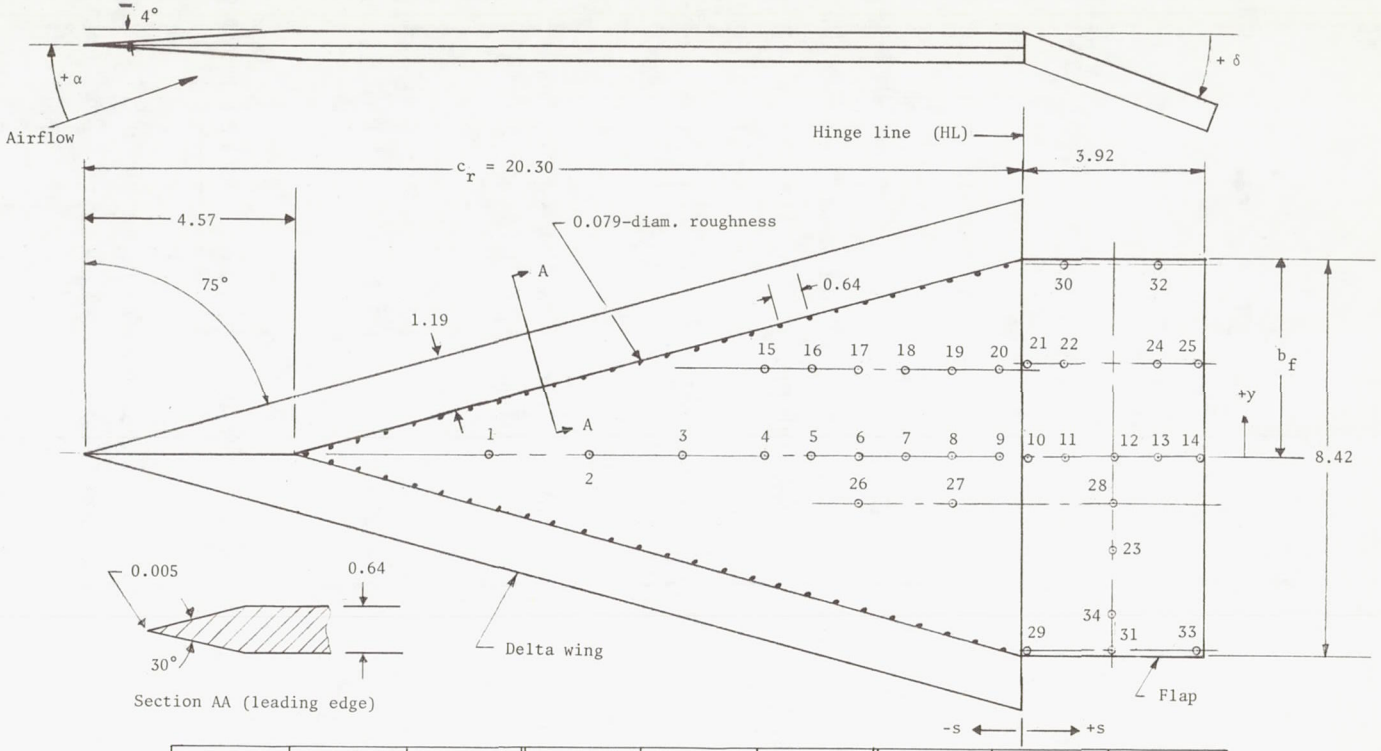

Orifice	s/c_r	y/b_f	Orifice	s/c_r	y/b_f	Orifice	s/c_r	y/b_f
1	-0.563	0	13	0.145	0	25	0.187	0.510
2	-.462	↓	14	.187	↓	26	-.175	-.240
3	-.363		15	-.275	.456	27	-.075	-.240
4	-.275		16	-.225	↓	28	.097	-.226
5	-.226		17	-.175		29	.007	-.962
6	-.174		18	-.125		30	.048	.962
7	-.125		19	-.075		31	.097	-.962
8	-.075		20	-.024		32	.146	.962
9	-.025		21	.007	.494	33	.187	-.962
10	.007		22	.046	.494	34	.097	-.804
11	.048		23	.097	-.468			
12	.096	↓	24	.147	.510			

(a) Orifice locations on pressure model.

Figure 1.- Sketches of wing showing location of pressure orifices and thermocouples. All dimensions are in centimeters.

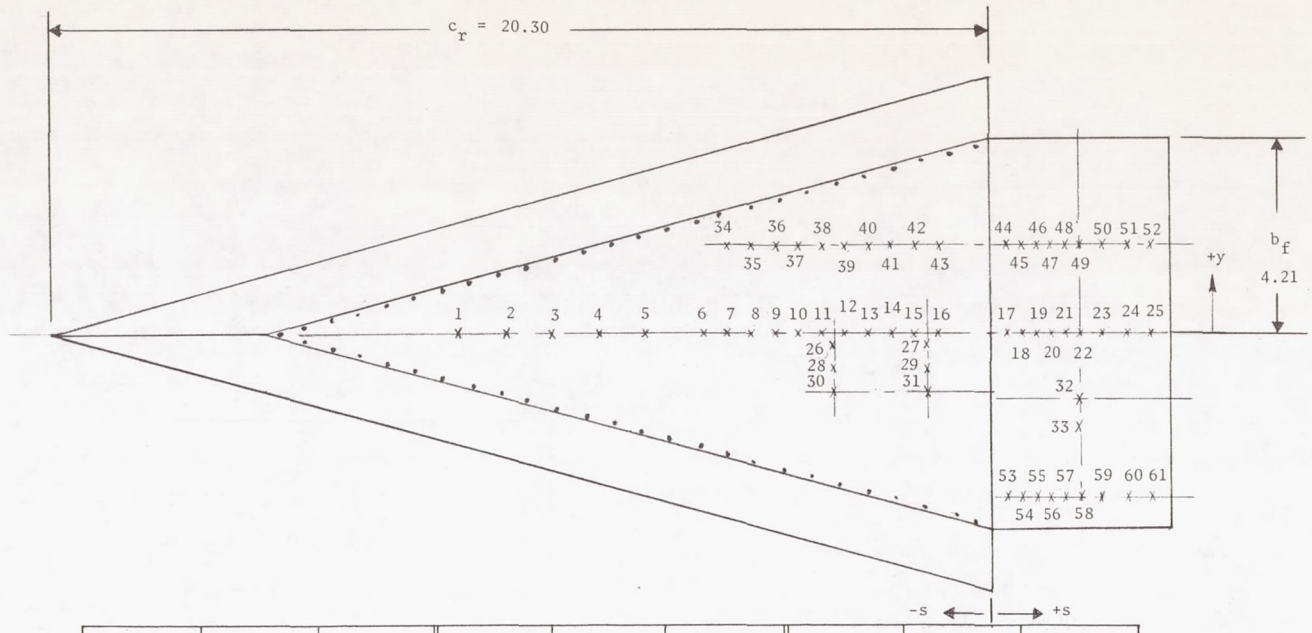

Thermocouple	s/c_r	y/b_f	Thermocouple	s/c_r	y/b_f	Thermocouple	s/c_r	y/b_f
1	-0.568	0	22	0.097	0	43	-0.056	0.452
2	-.518	↓	23	.122	↓	44	.019	↓
3	-.468		24	.147		45	.034	
4	-.418		25	.172		46	.050	
5	-.368		26	-.168	-.060	47	.066	
6	-.306		27	-.068	-.060	48	.081	
7	-.305		28	-.168	-.180	49	.097	
8	-.255		29	-.068	-.180	50	.122	
9	-.231		30	-.168	-.302	51	.147	
10	-.206		31	-.068	-.302	52	.172	
11	-.180		32	.097	-.332	53	.019	-.844
12	-.156		33	.097	-.482	54	.034	↓
13	-.131		34	-.281	.452	55	.050	
14	-.106		35	-.256	↓	56	.066	
15	-.081		36	-.231		57	.081	
16	-.056		37	-.206		58	.097	
17	.002		38	-.181		59	.121	
18	.034		39	-.156		60	.147	
19	.050		40	-.131		61	.172	
20	.066		41	-.106				
21	.081	↓	42	-.081	↓			

(b) Thermocouple locations on heat-transfer model.

Figure 1.- Concluded.

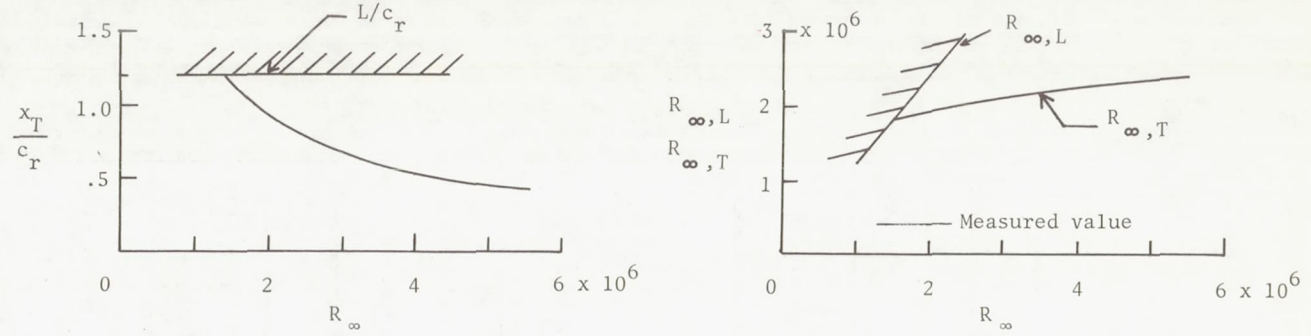

(a) Transition movement with free-stream Reynolds number. $\alpha = 0^0$.

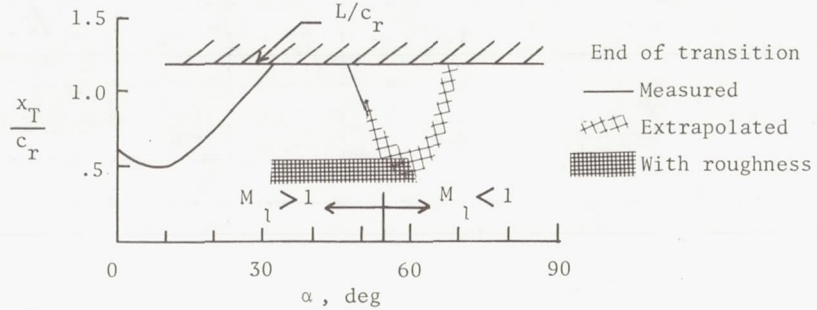

(b) Transition movement with angle of attack. $R_\infty \approx 3.4 \times 10^6$.

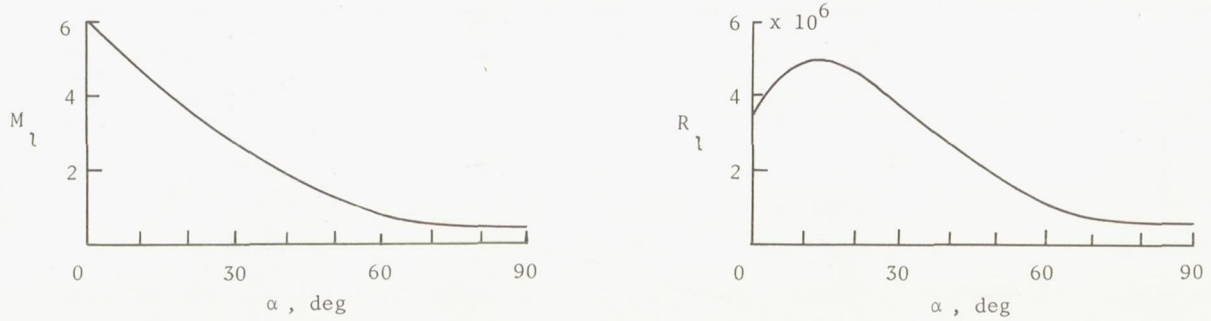

(c) Local Mach number and Reynolds number. $R_\infty \approx 3.4 \times 10^6$.

Figure 2.- Local conditions and movement of end of transition on center line of delta wing and flap. $\delta = 0^0$.

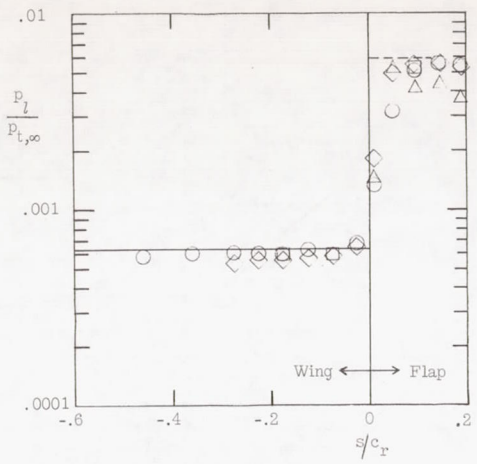

(a) $\alpha = 0^0$. Calculated hypersonic flow on wing and supersonic flow on flap.

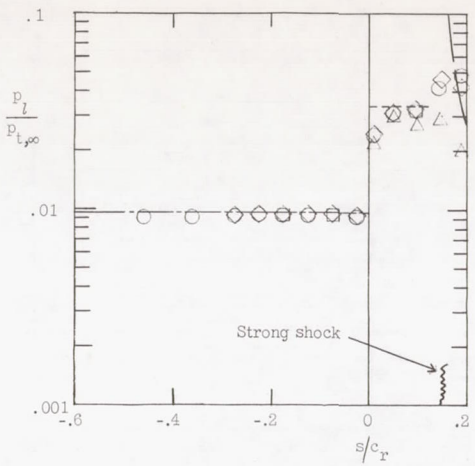

(b) $\alpha = 30^0$. Calculated supersonic flow on wing and flap.

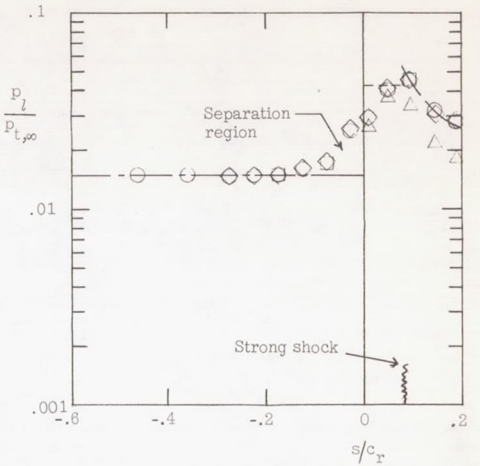

(c) $\alpha = 40^0$. Calculated supersonic flow on wing and flap.

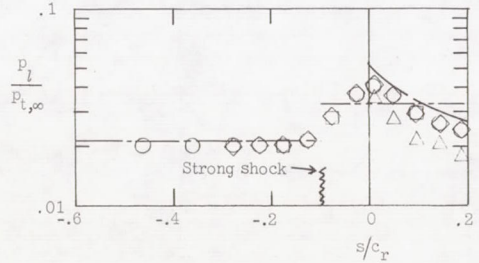

(d) $\alpha = 50^0$. Calculated supersonic flow on wing and subsonic flow on flap.

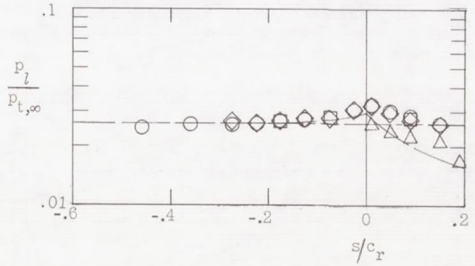

(e) $\alpha = 60^0$. Calculated subsonic flow on wing and flap.

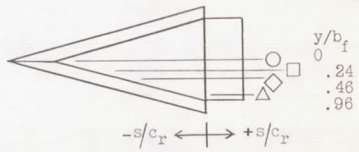

——— p_∞ for $M_\infty = 6$
– – – – Inviscid pressure (1 shock)
——— Tangent cone
——— Static pressure behind normal shock ($M_1 = 1.23$)
——— Static pressure behind normal shock ($M_\infty = 6$)
———— Subsonic parabolic pressure distribution (ref. 9)

L-695244

Figure 3.- Typical pressure distribution on delta wing for various flow regimes. Free-stream airflow direction is indicated on schlieren photographs by arrows. $\delta = 20^0$; $R_\infty \approx 3.4 \times 10^6$.

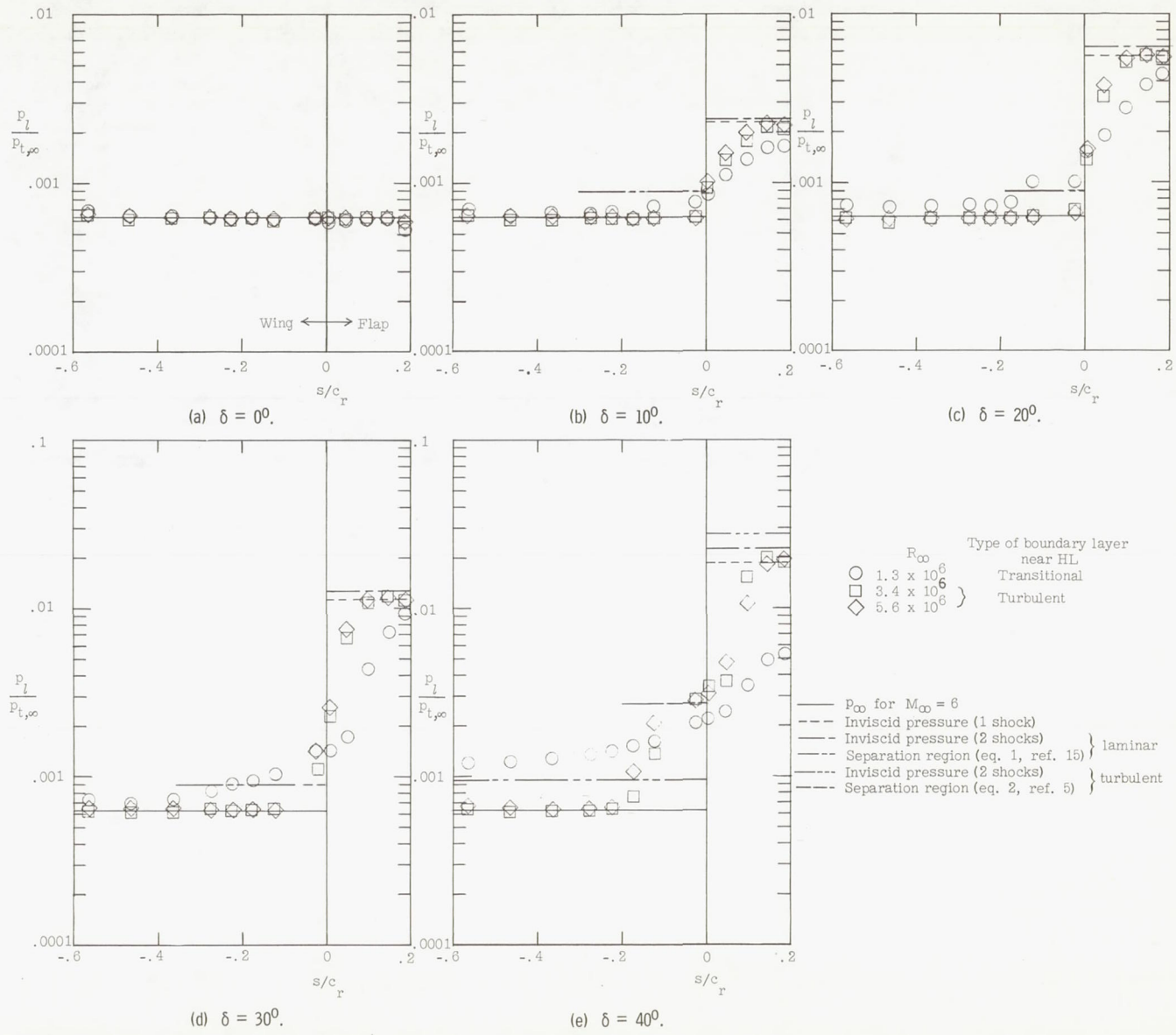

Figure 4.- Effect of Reynolds number on the pressure distribution along the center line for various flap deflection angles at $\alpha = 0^\circ$.

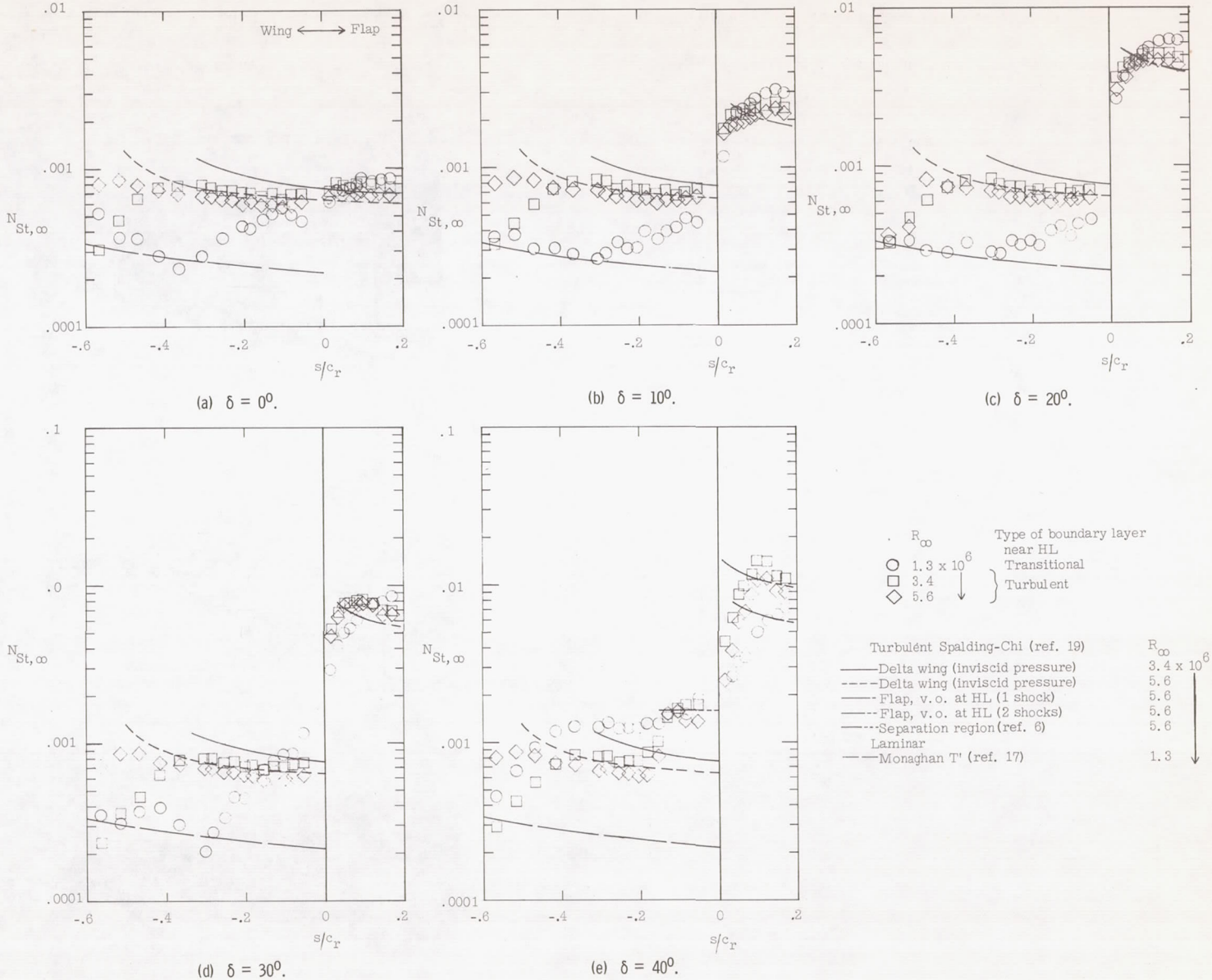

Figure 5.- Effect of Reynolds number on the Stanton number distribution along the center line for various flap deflection angles at $\alpha = 0^\circ$.

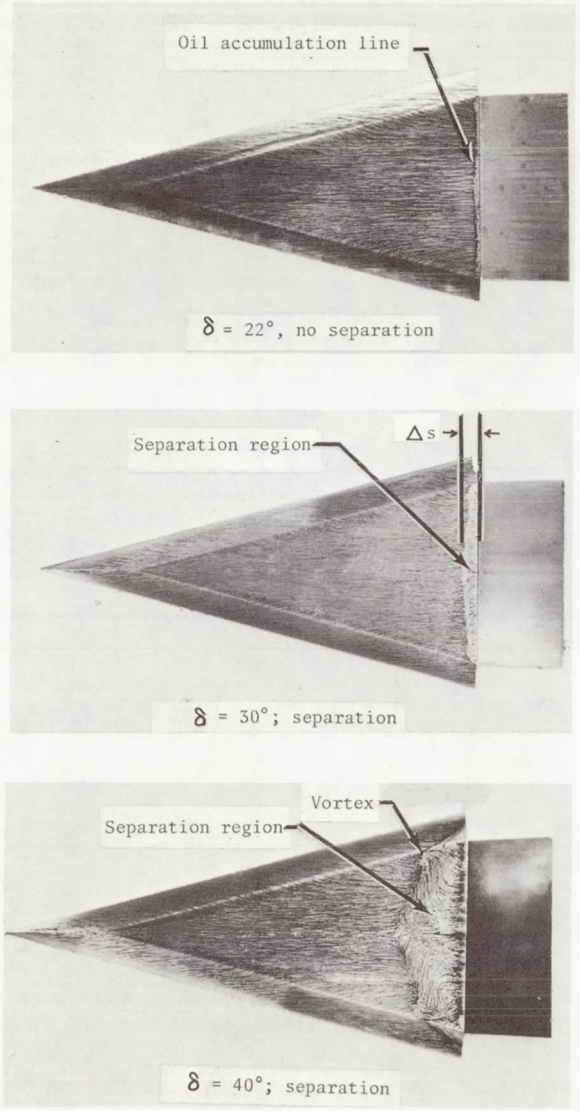

(a) Typical oil-flow patterns, $R_\infty = 5.6 \times 10^6$.

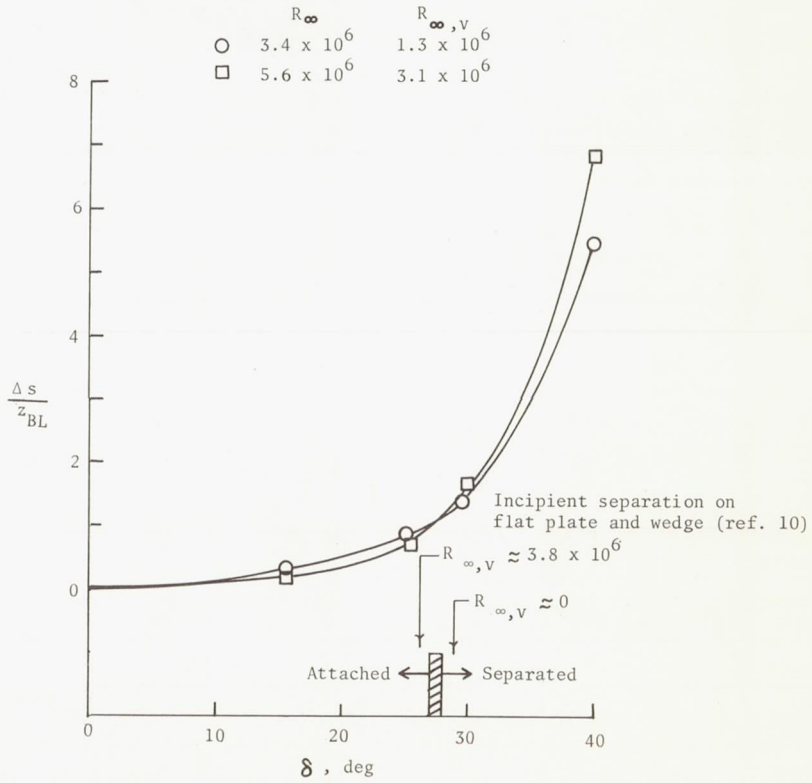

(b) Variation of oil-accumulation line with flap deflection angle.

Figure 6.- Turbulent separation at zero angle of attack.

L-69-5245

(a) $\delta = 0^{o}$.

(b) $\delta = 10^{o}$.

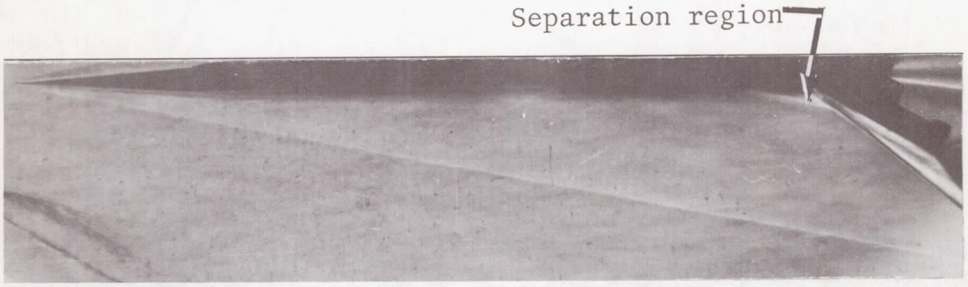

(c) $\delta = 30^{o}$.

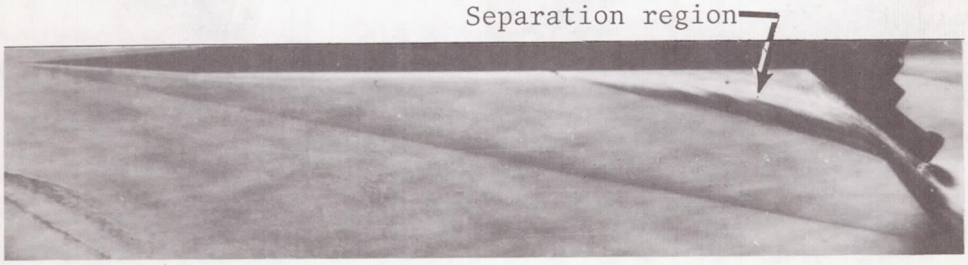

(d) $\delta = 40^{o}$. L-69-5246

Figure 7.- Typical schlieren photographs at $\alpha = 0^{o}$ for turbulent flow. $R_{\infty} \approx 3.4 \times 10^{6}$.

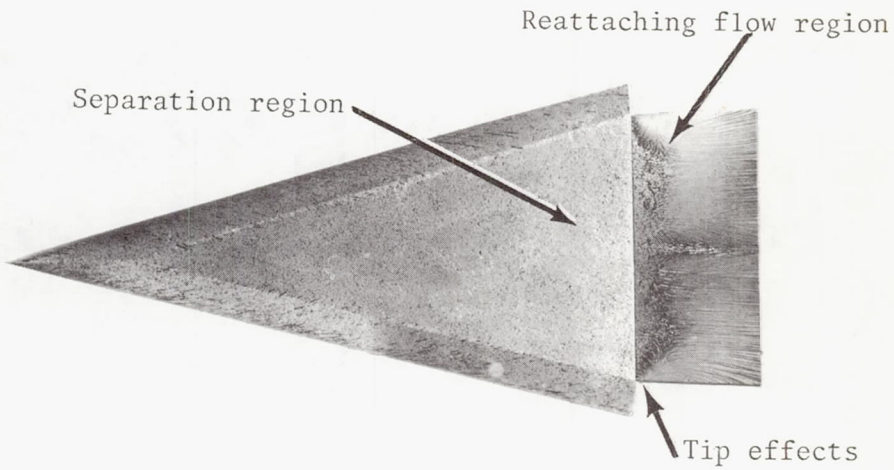

(a) Oil-flow pattern.

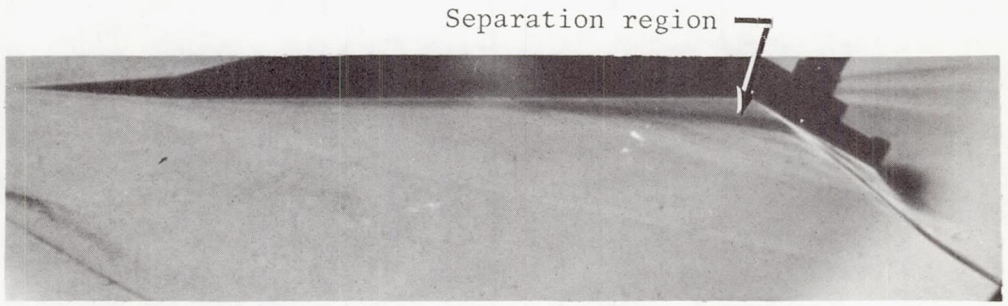

(b) Schlieren photograph. L-69-5247

Figure 8.- Transitional separation. $\alpha = 0^{o}$; $\delta = 30^{o}$; $R_{\infty} \approx 1.3 \times 10^{6}$.

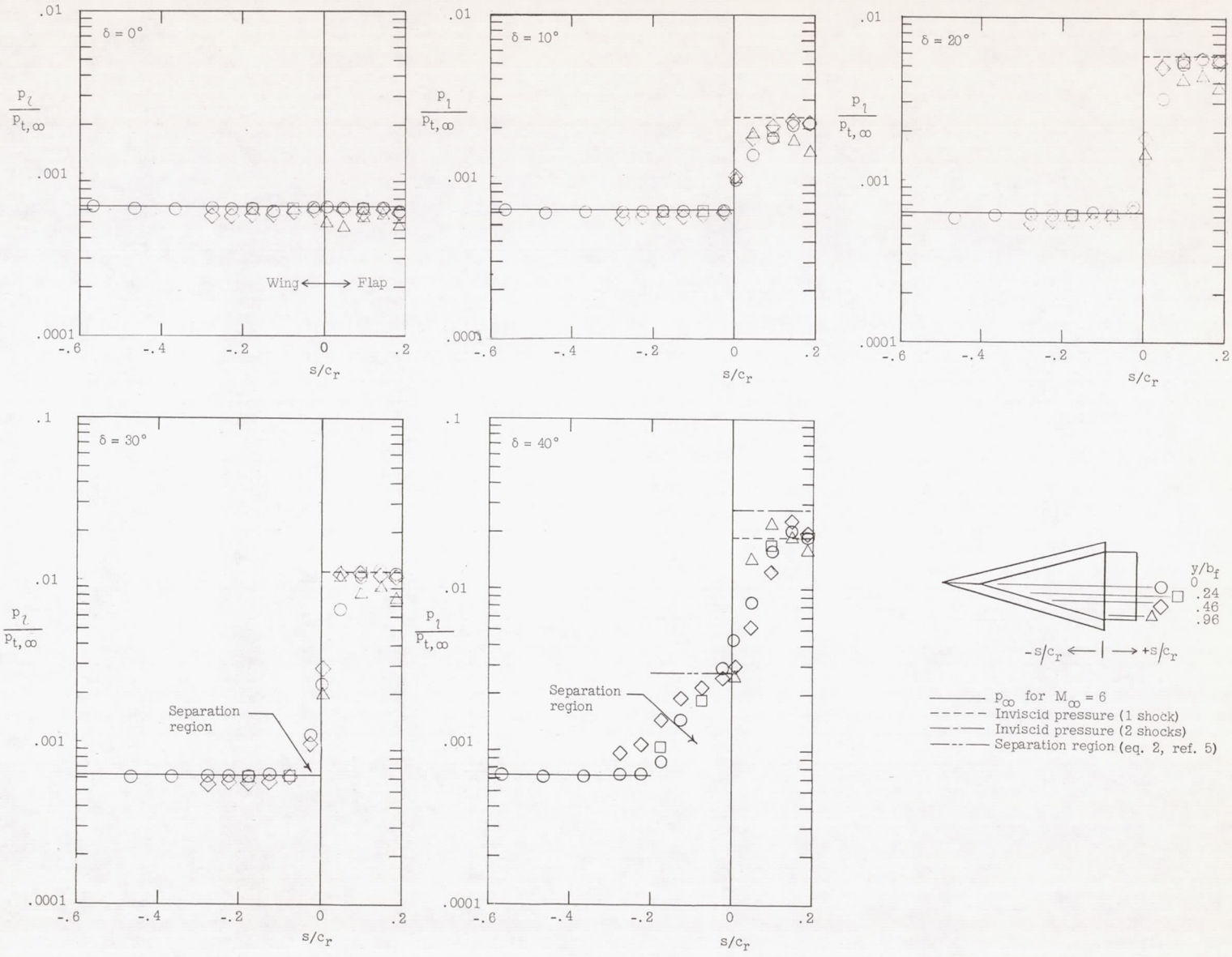

(a) $\alpha = 0^0$.

Figure 9.- Spanwise variation of pressure distributions on the delta wing and flap at low angles of attack for several flap deflection angles. $R_\infty \approx 3.4 \times 10^6$.

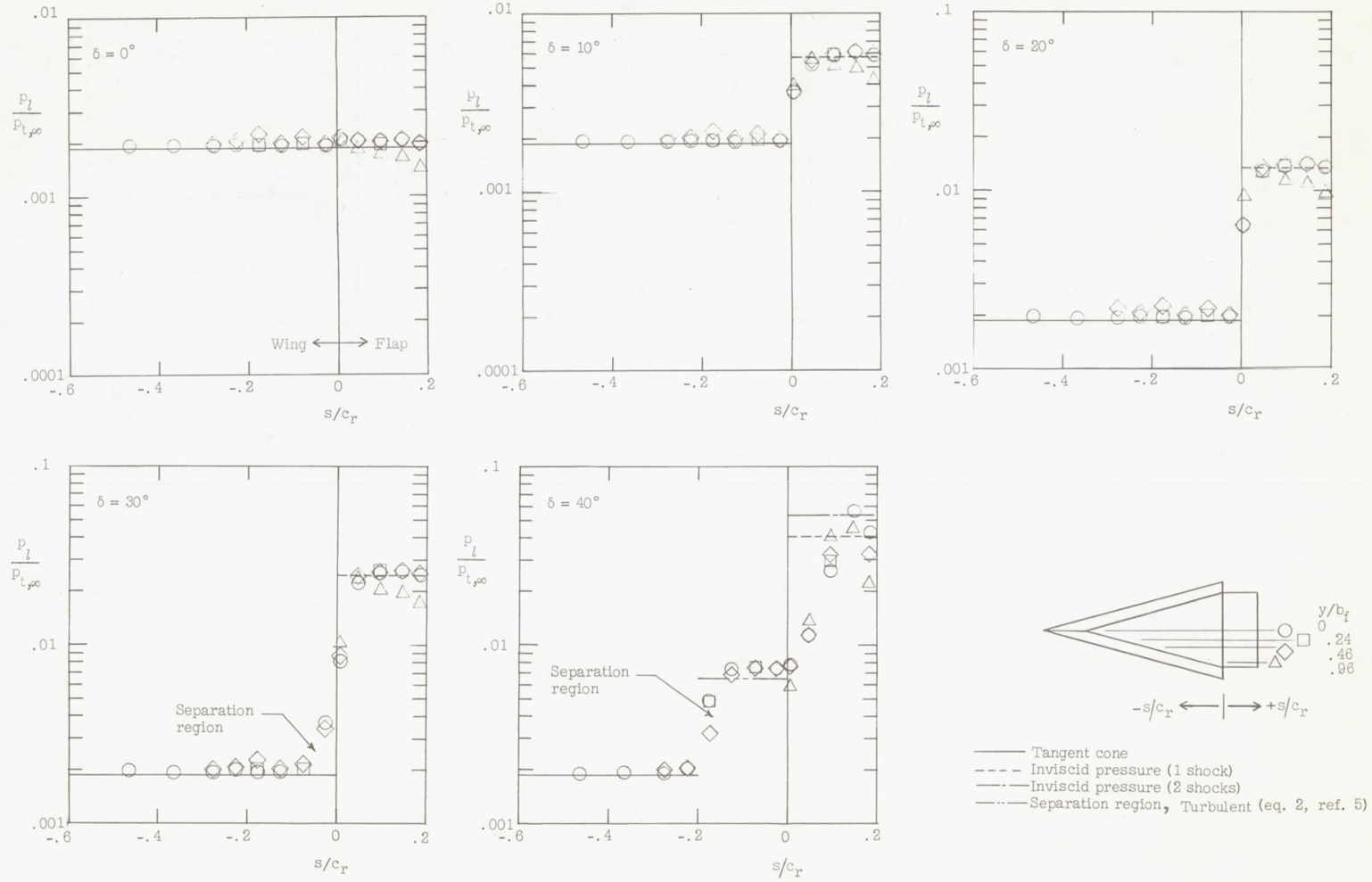

(b) $\alpha = 10^0$.

Figure 9.- Concluded.

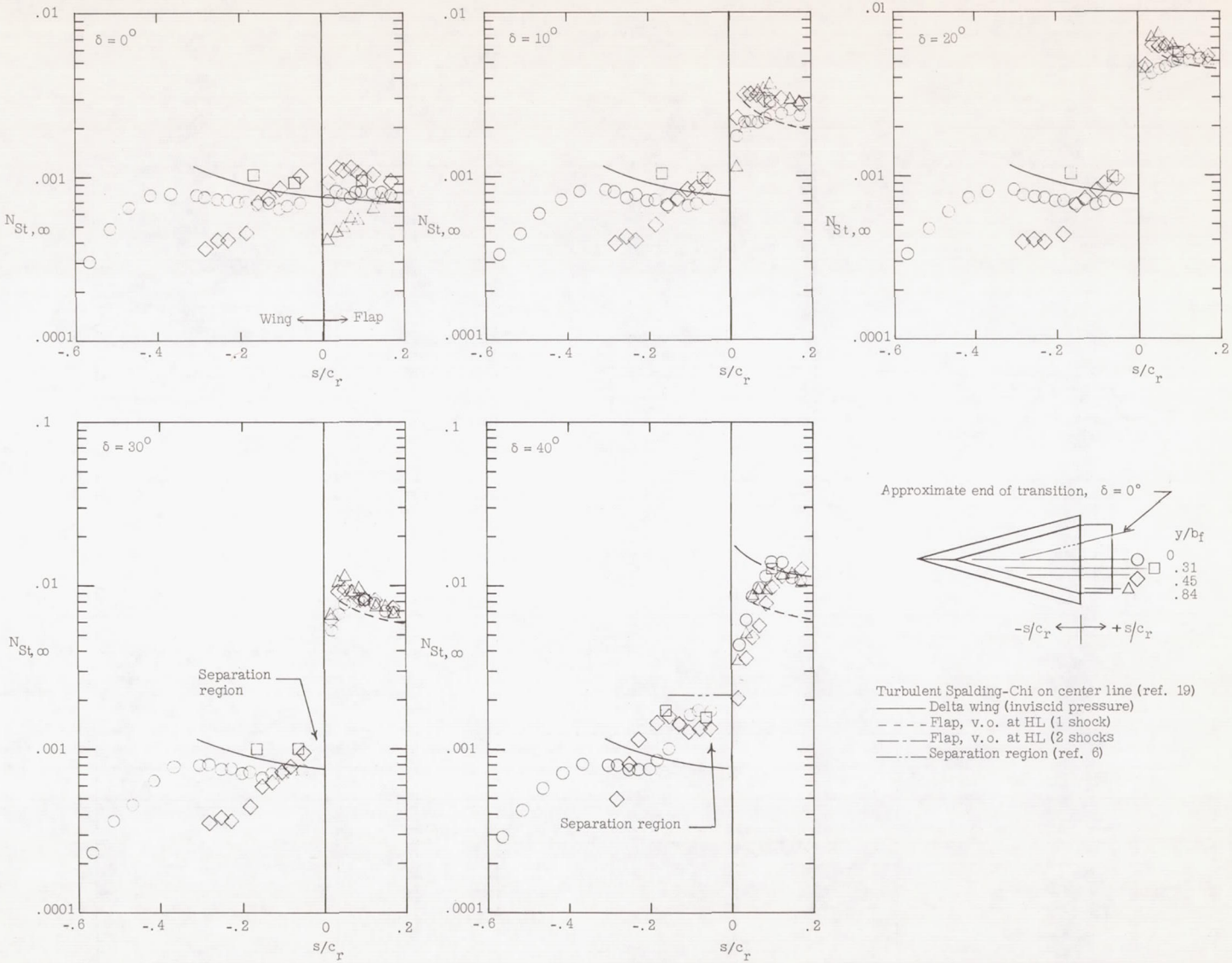

(a) $\alpha = 0^0$.

Figure 10.- Spanwise variation of heat transfer on the wing and flap at an angle of attack for several flap deflection angles. $R_\infty \approx 3.4 \times 10^6$.

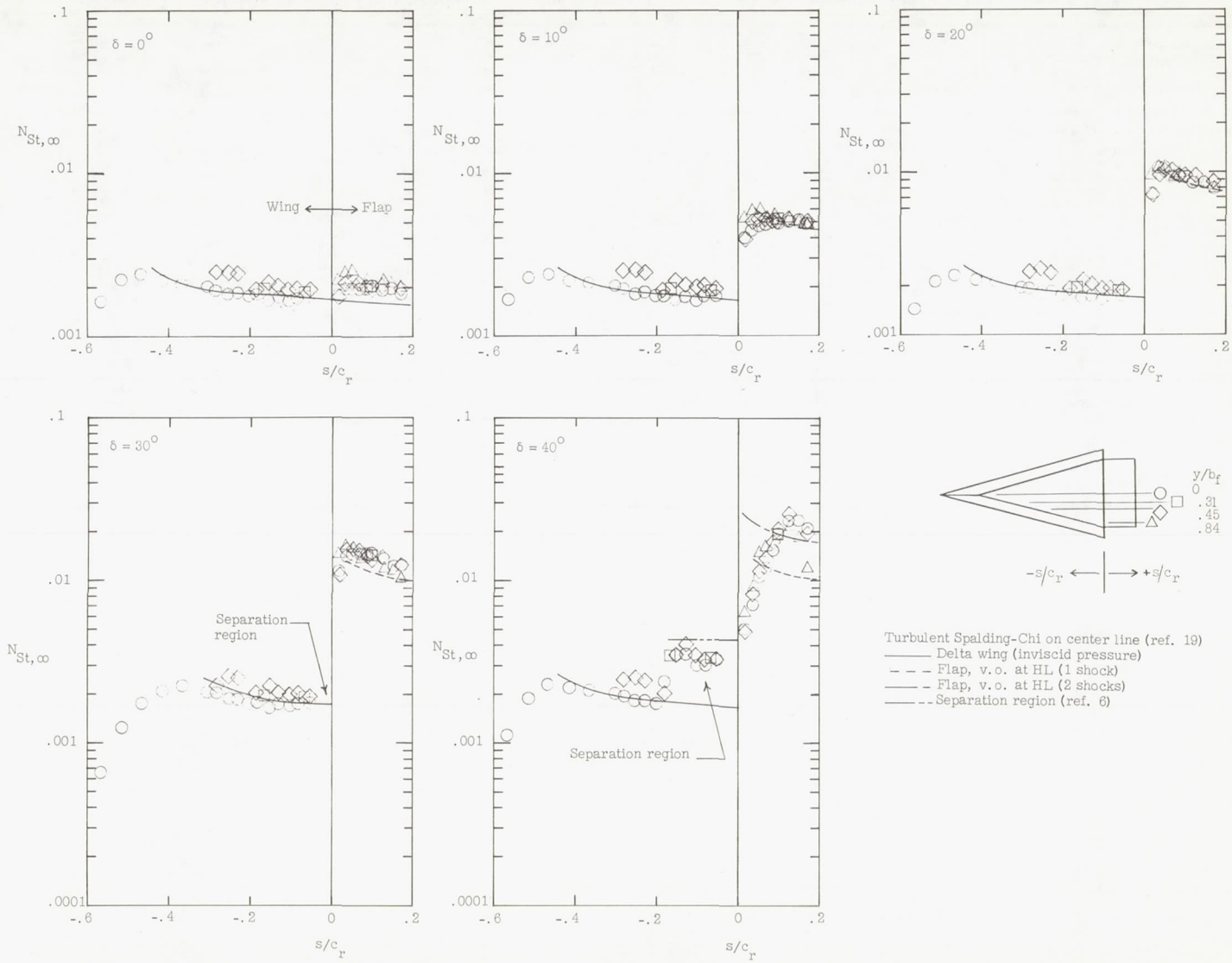

(b) $\alpha = 10^{o}$.

Figure 10.- Concluded.

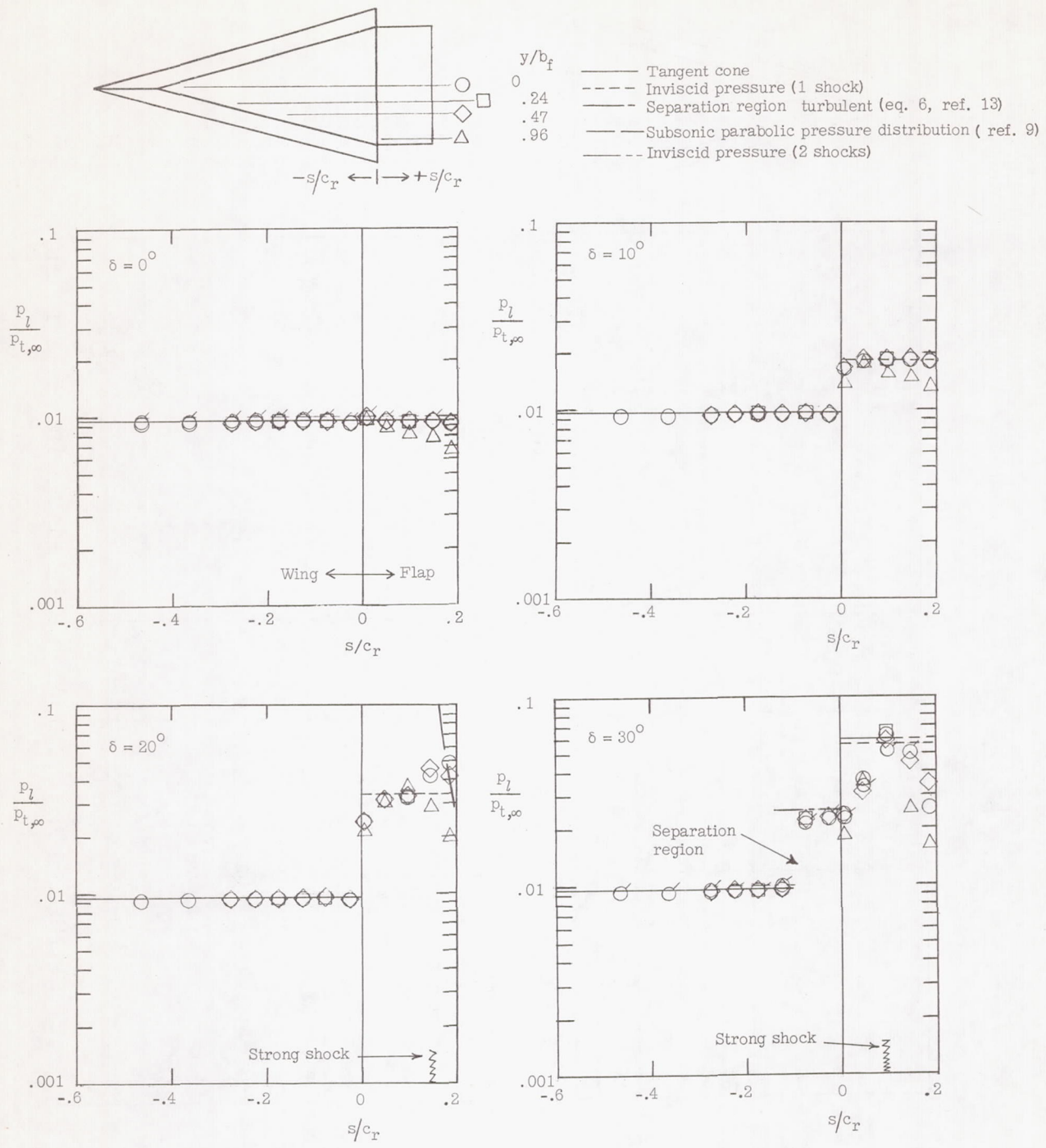

(a) $\alpha = 30^{0}$.

Figure 11.- Pressure distribution on wing and flap at the moderate angles of attack for various spanwise stations. $R_{\infty} \approx 3.4 \times 10^{6}$. Flagged symbols indicate center-line data obtained on model with roughness.

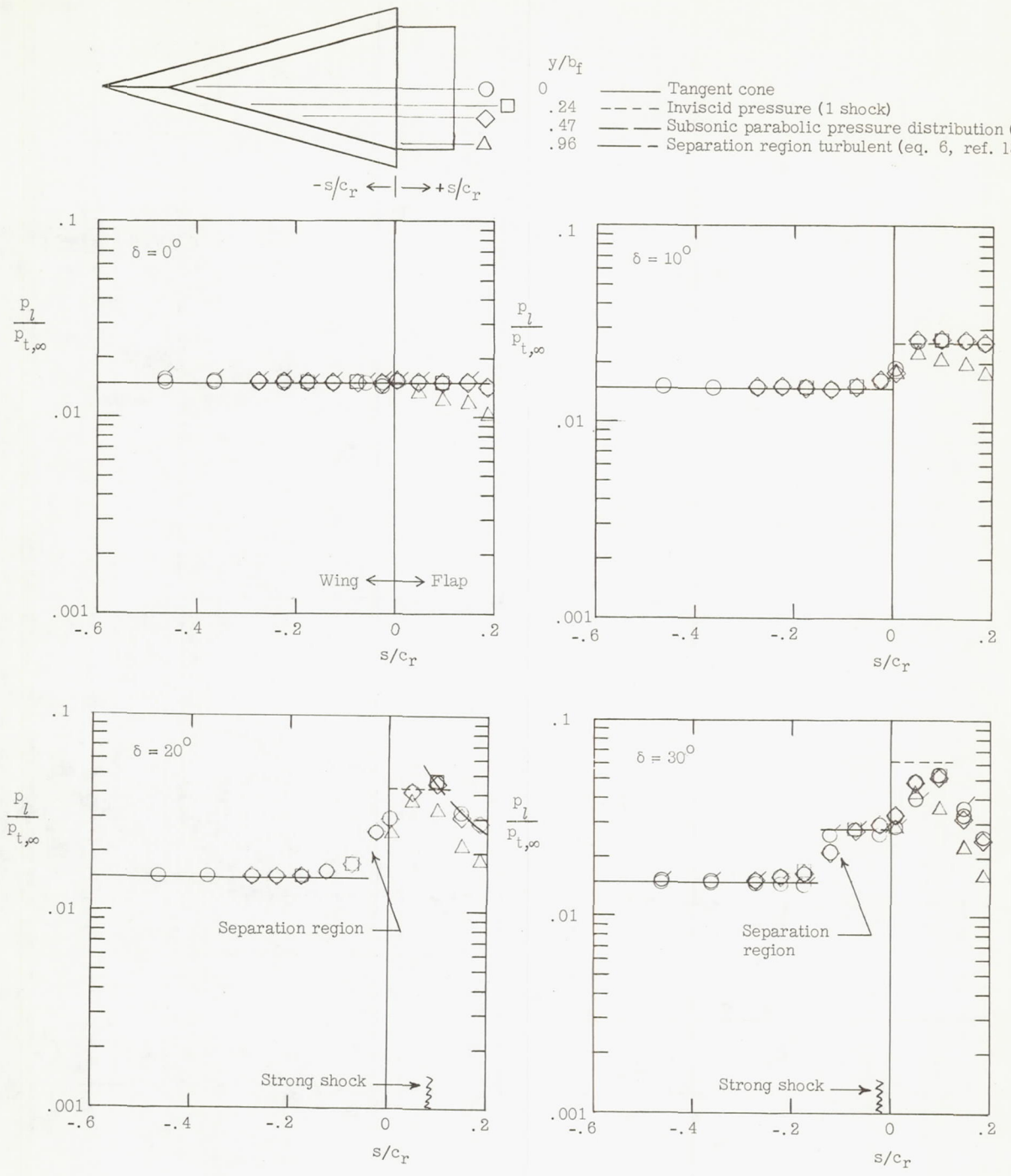

(b) $\alpha = 40^\circ$.

Figure 11.- Continued.

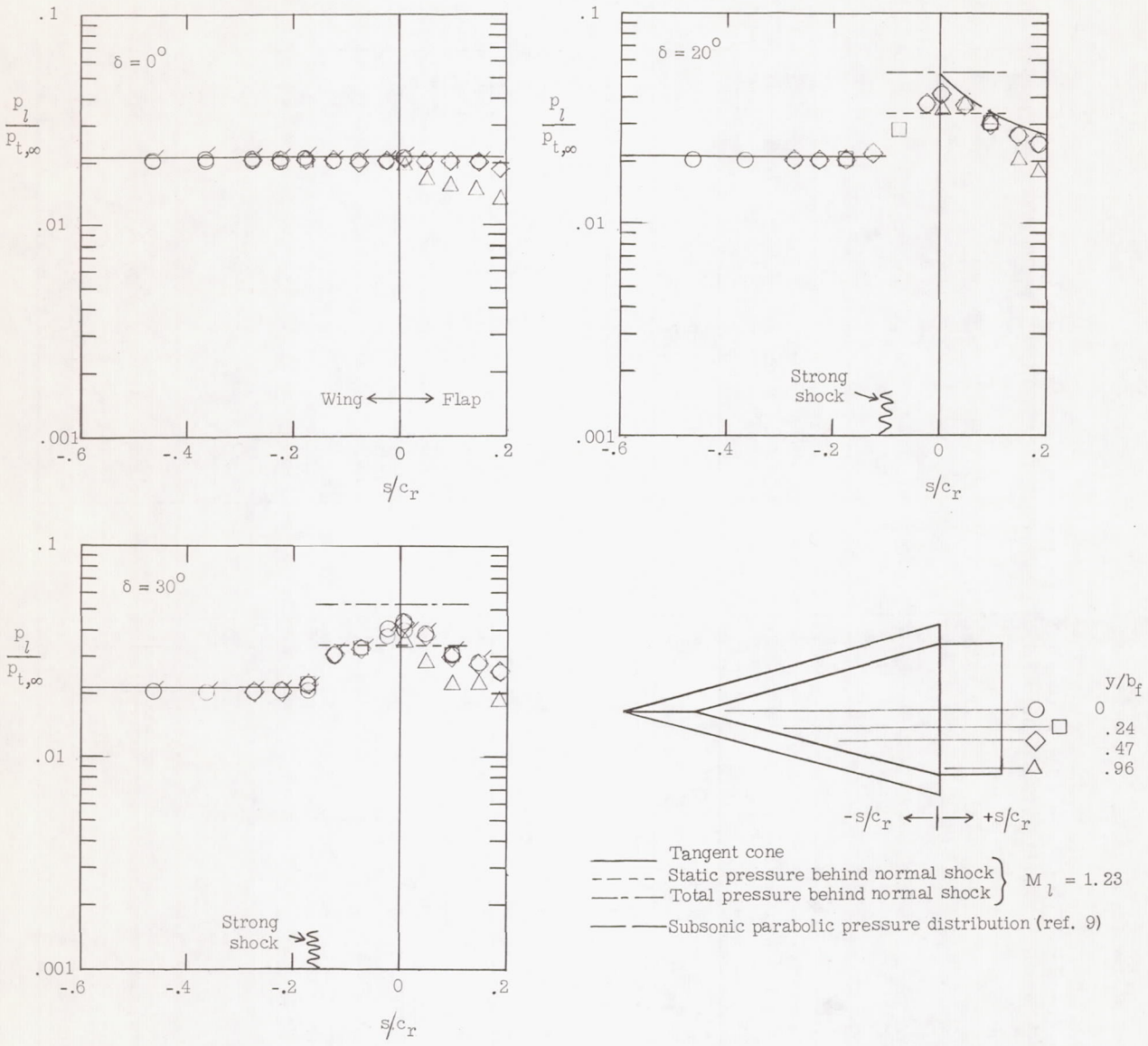

(c) $\alpha = 50^{\circ}$.

Figure 11.- Concluded.

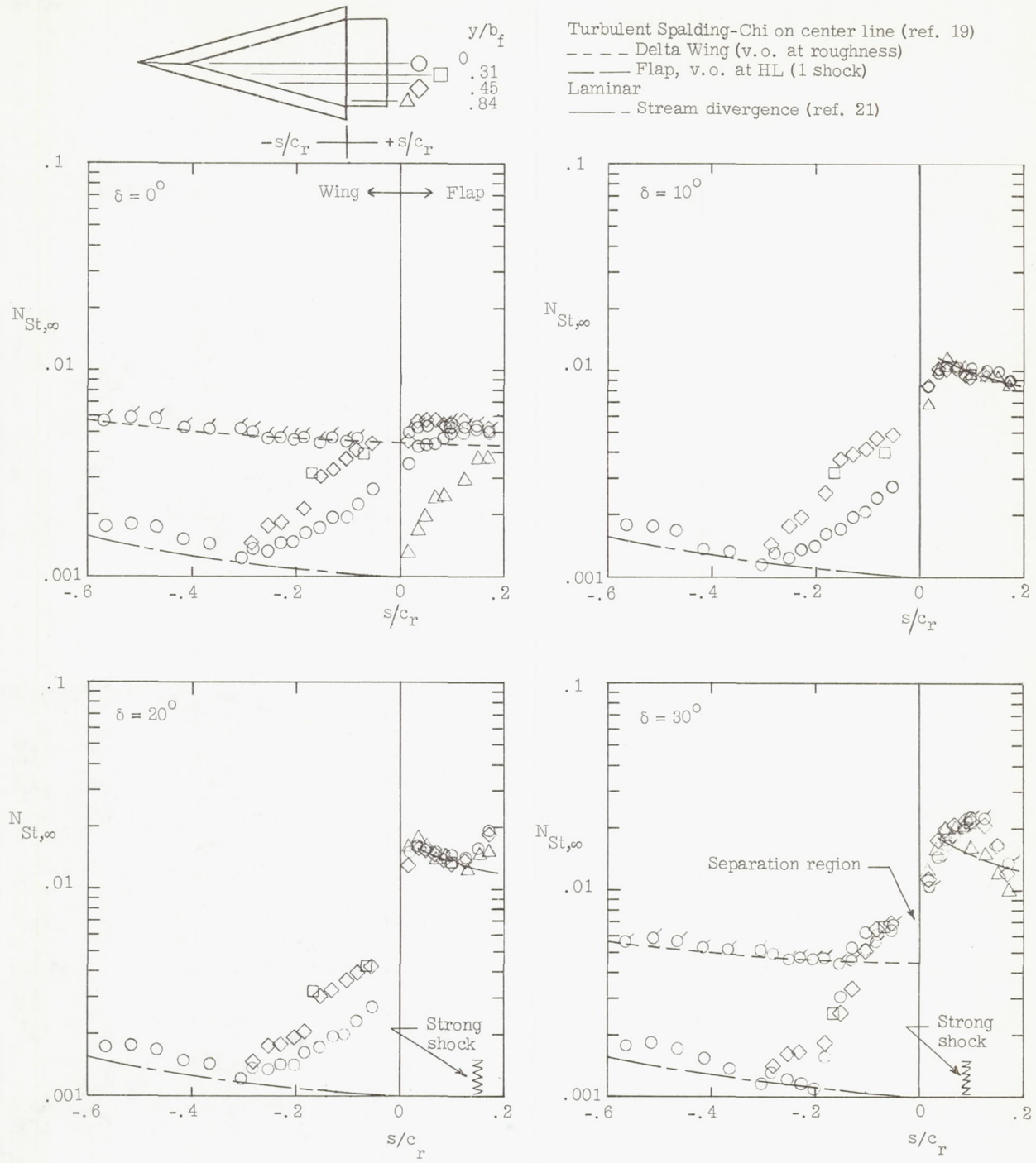

(a) $\alpha = 30^{\circ}$.

Figure 12.- Typical heat transfer on wing and flaps at moderate angles of attack for various spanwise stations. $R_{\infty} \approx 3.4 \times 10^{6}$. Flagged symbols indicate center-line data obtained on model with roughness.

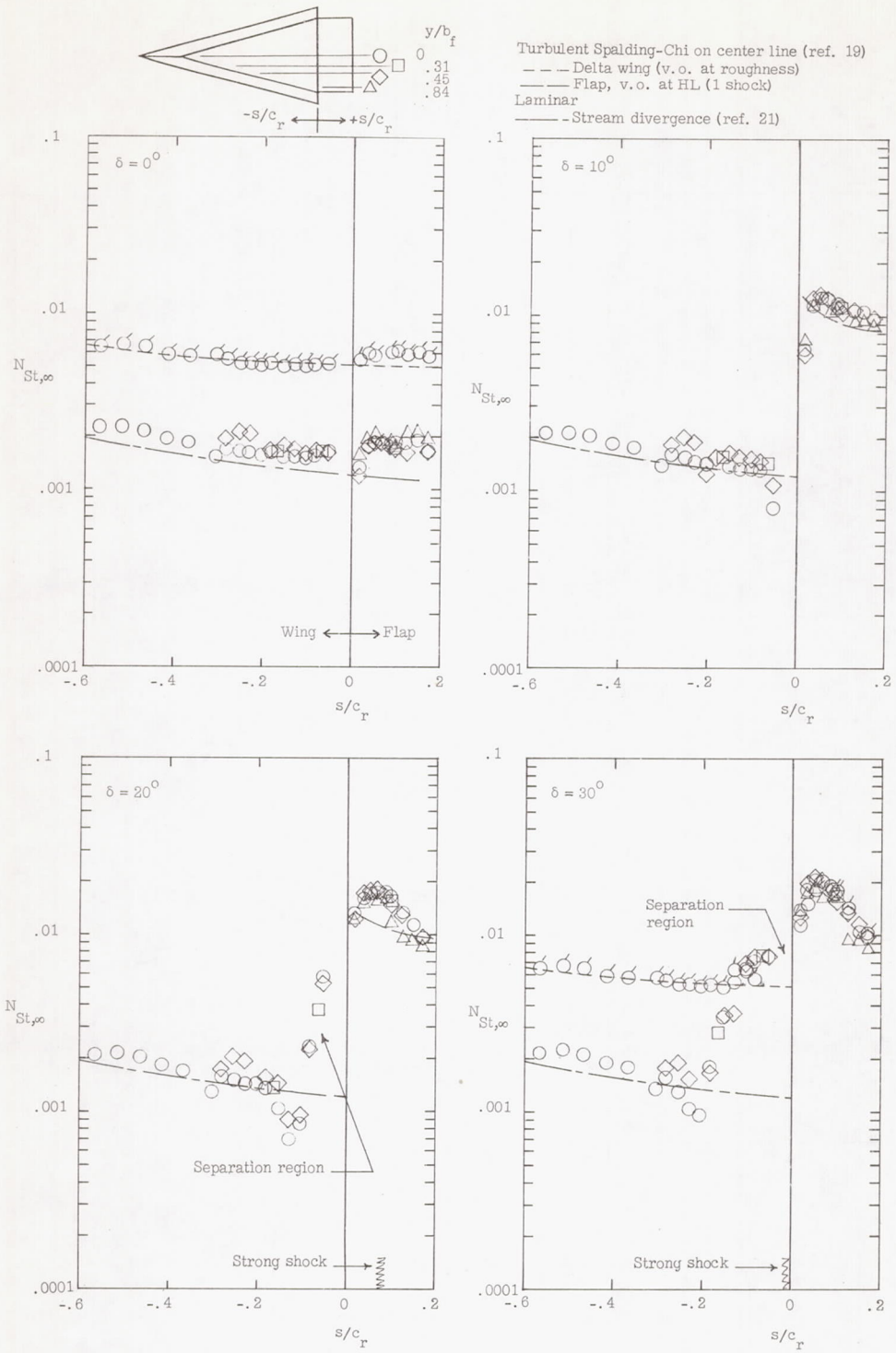

(b) $\alpha = 40^{0}$.

Figure 12.- Continued.

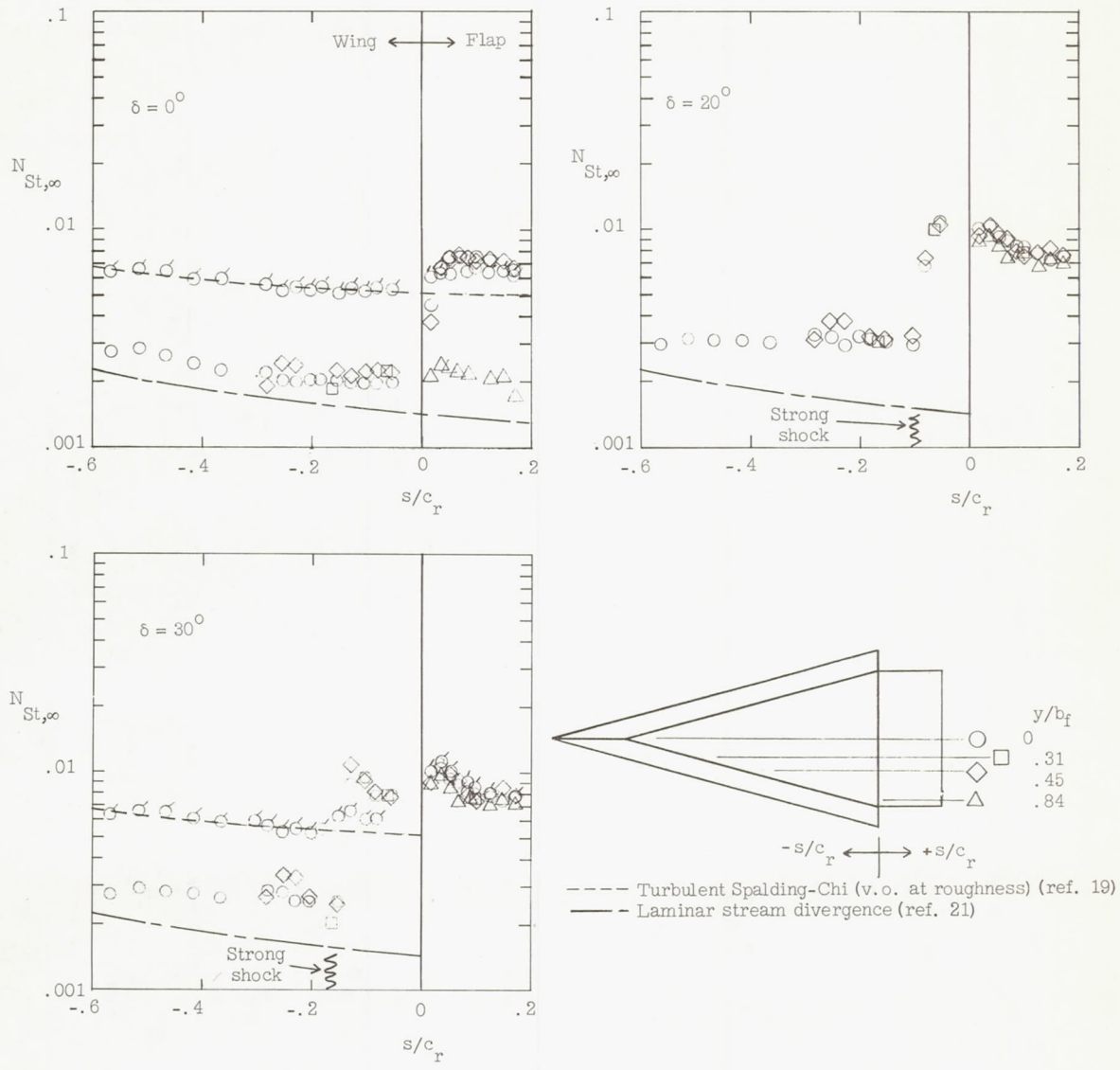

(c) $\alpha = 50^{0}$.

Figure 12.- Concluded.

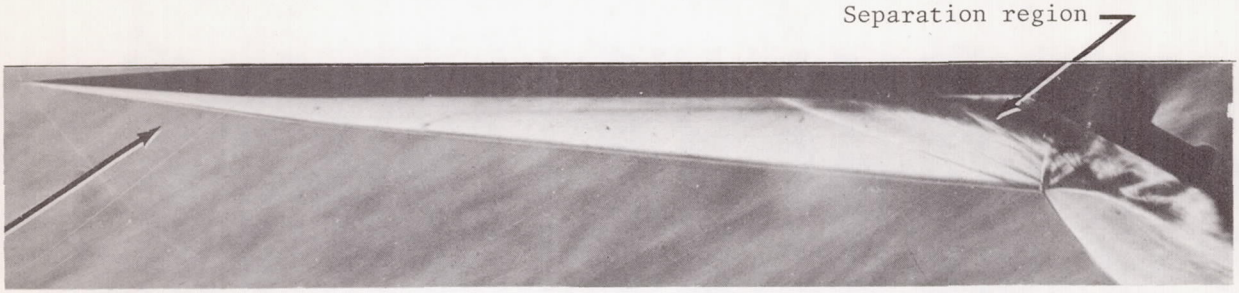

(a) $\alpha = 30^{o}$.

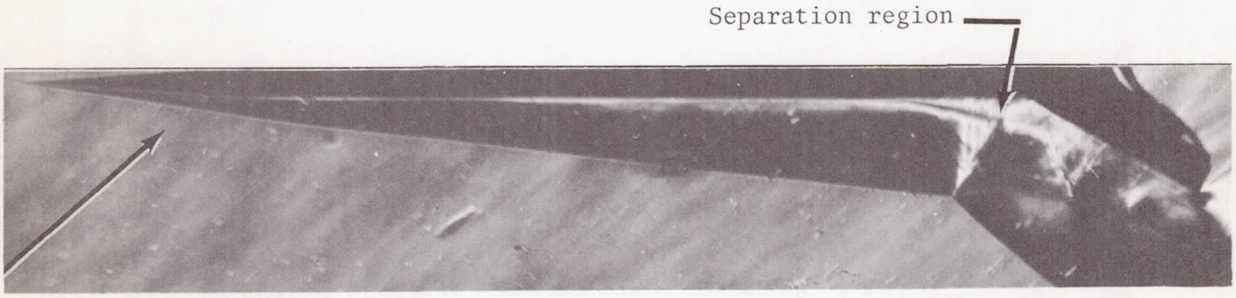

(b) $\alpha = 40^{o}$.

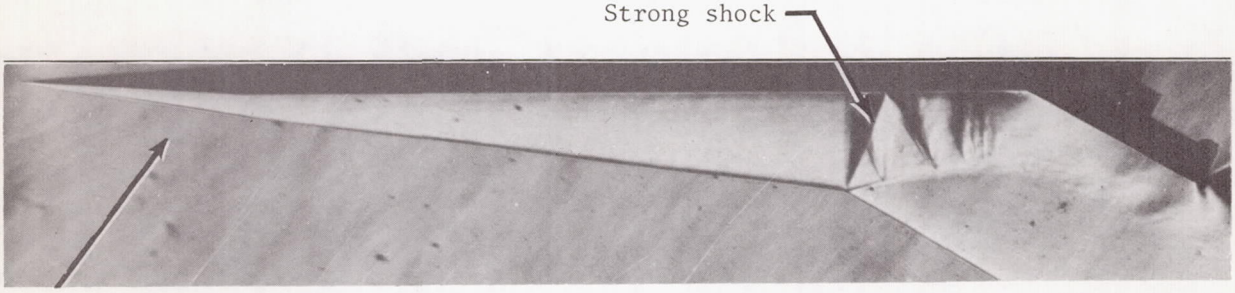

(c) $\alpha = 50^{o}$.

L-69-5248

Figure 13.- Typical schlieren photographs for the moderate angles of attack. Free-stream airflow direction is indicated by arrows. $\delta = 30^{o}$; $R_{\infty} \approx 3.4 \times 10^{6}$.

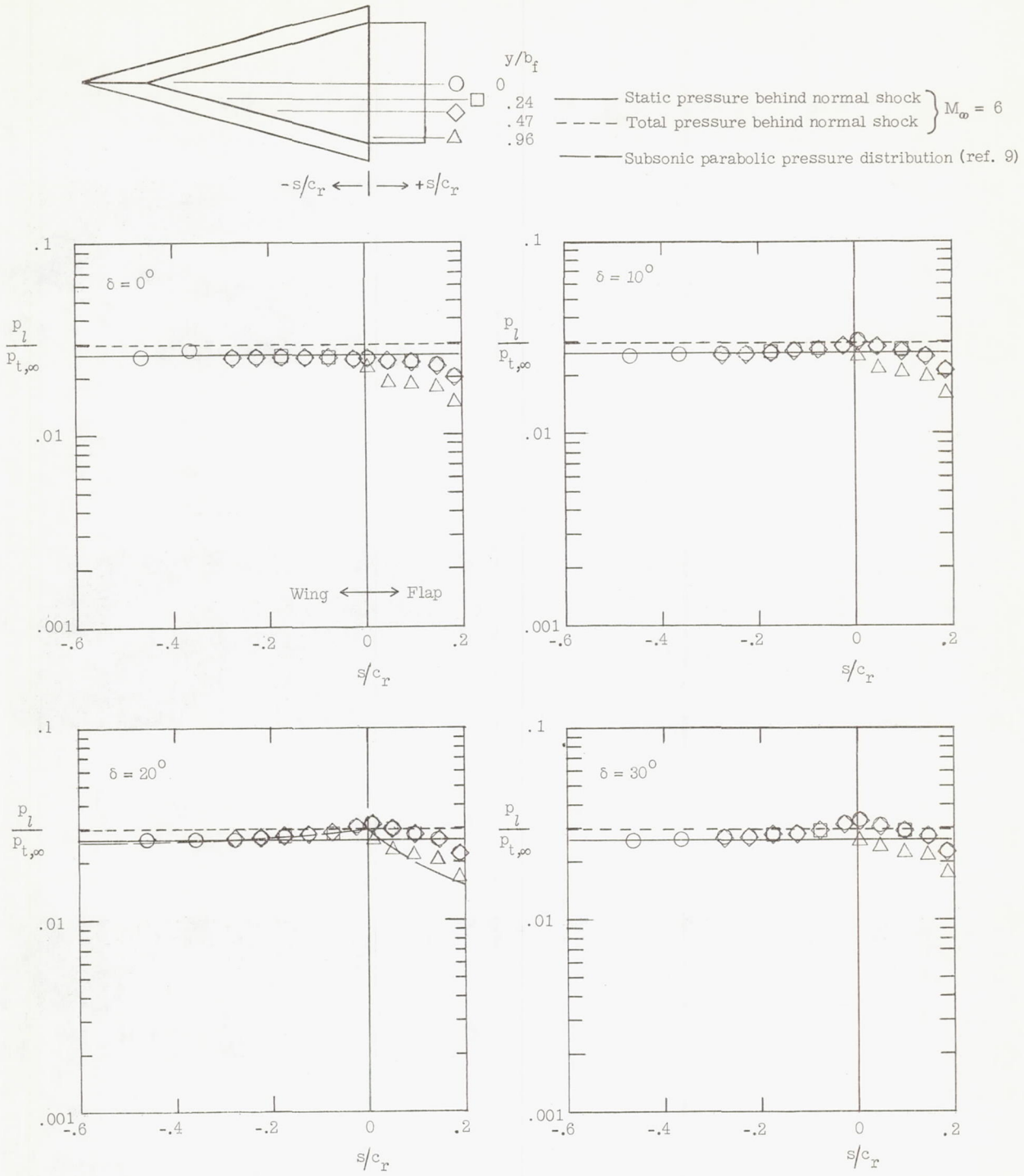

(a) $\alpha = 60^{0}$.

Figure 14.- Pressure distribution on the delta wing and flap at high angles of attack for various spanwise stations. Subsonic flow on delta wing and flap; $R_{\infty} \approx 3.4 \times 10^{6}$.

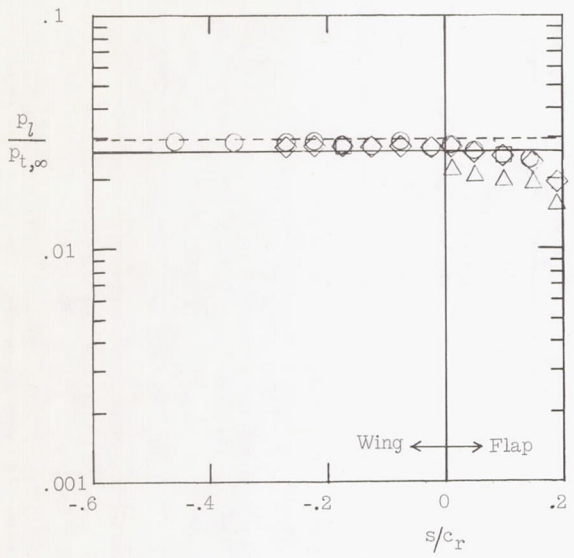

(b) $\alpha = 70^0$; $\delta = 0^0$.

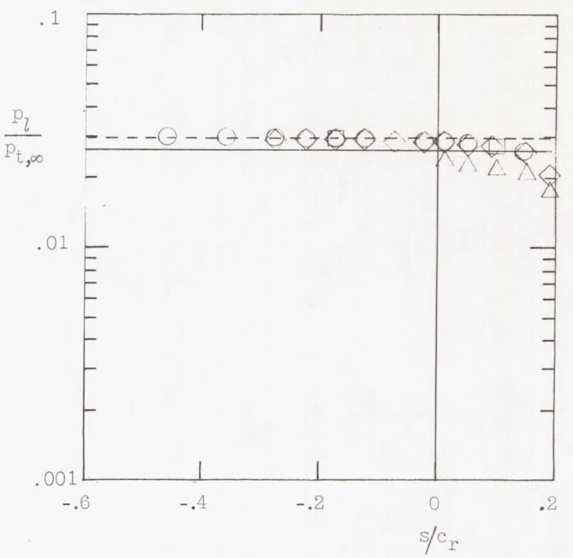

(c) $\alpha = 80^0$; $\delta = 0^0$.

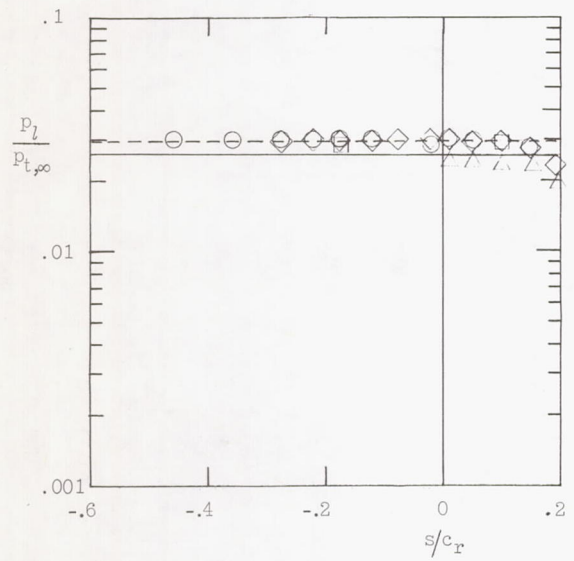

(d) $\alpha = 90^0$; $\delta = 0^0$.

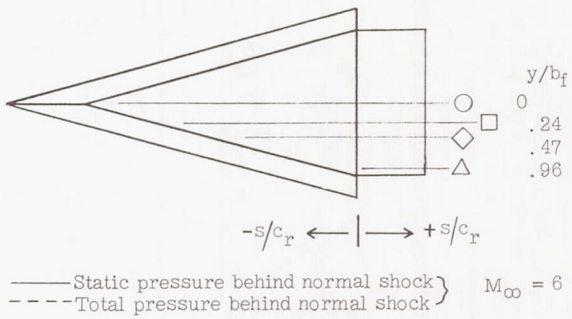

Figure 14.- Concluded.

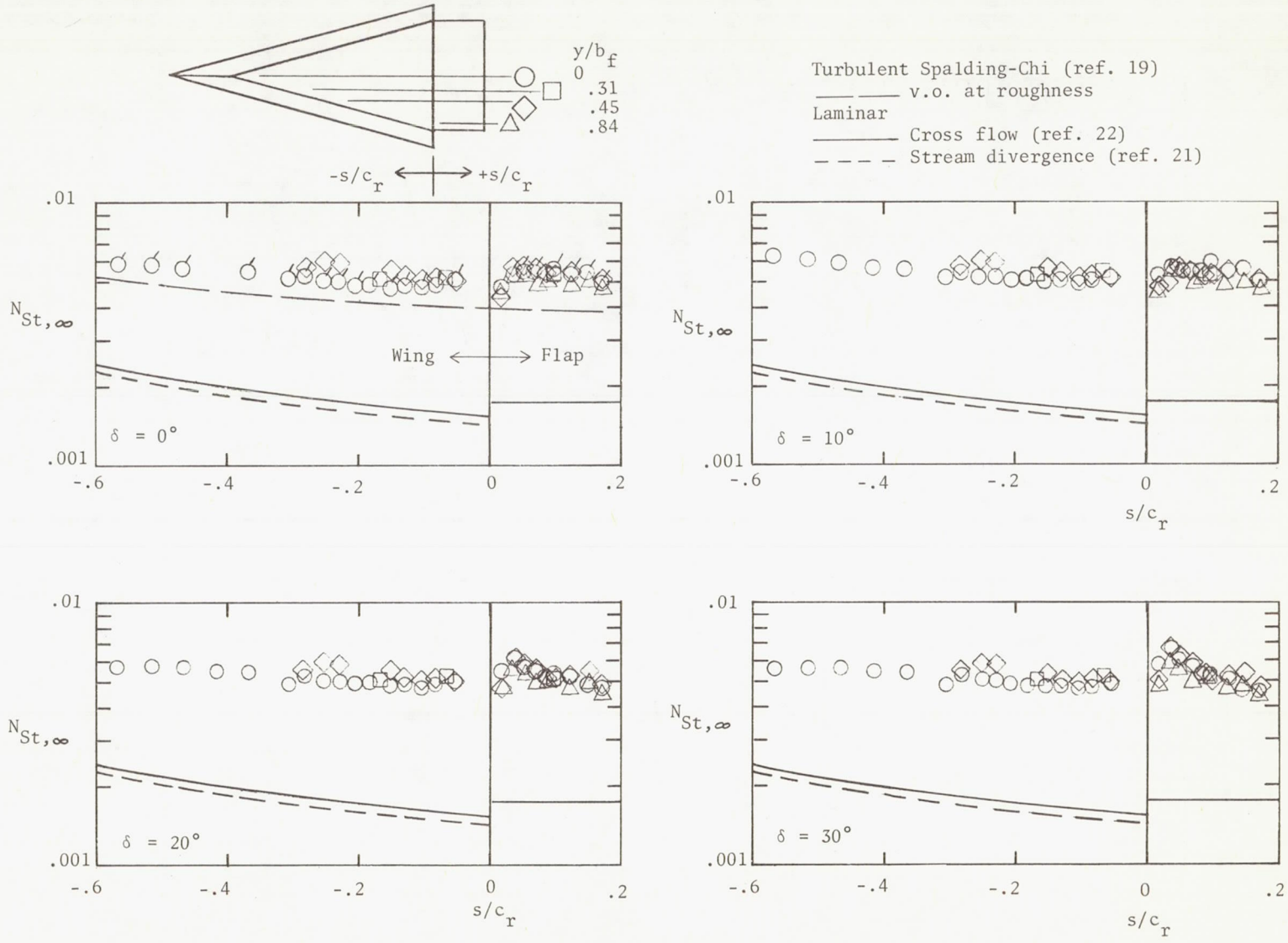

(a) $\alpha = 60^{0}$.

Figure 15.- Heat transfer on the delta wing and flap at high angles of attack for various spanwise stations. Subsonic flow on wing flap; $R_{\infty} \approx 3.4 \times 10^{6}$. Flagged symbols indicate center-line data obtained on model with roughness.

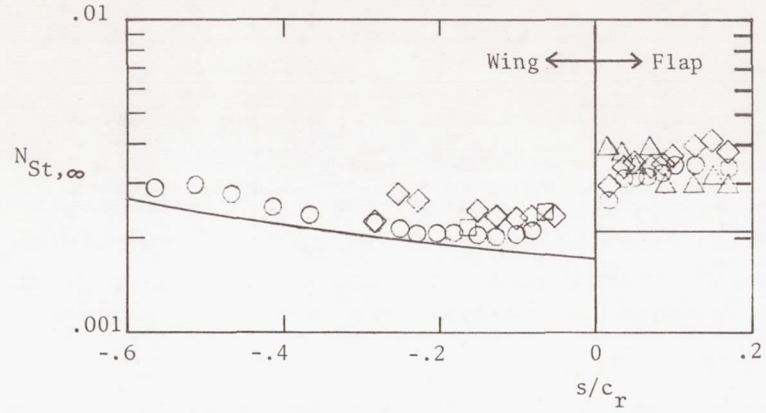

(b) $\alpha = 70^0$; $\delta = 0^0$.

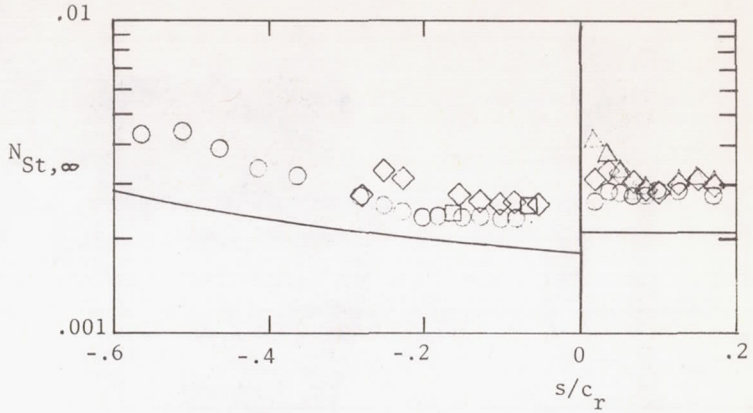

(c) $\alpha = 80^0$; $\delta = 0^0$.

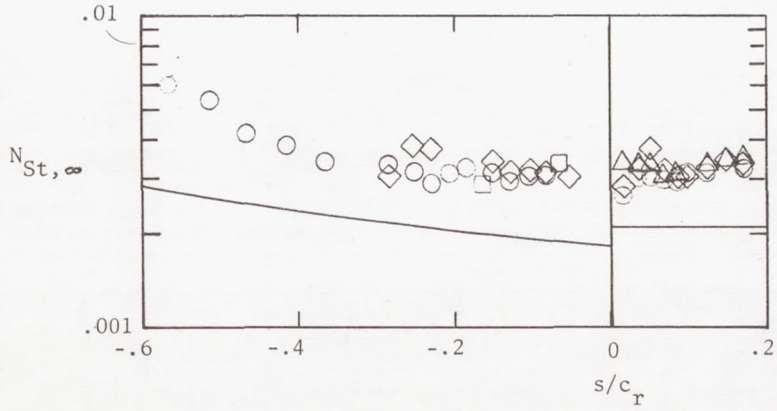

(d) $\alpha = 90^0$; $\delta = 0^0$.

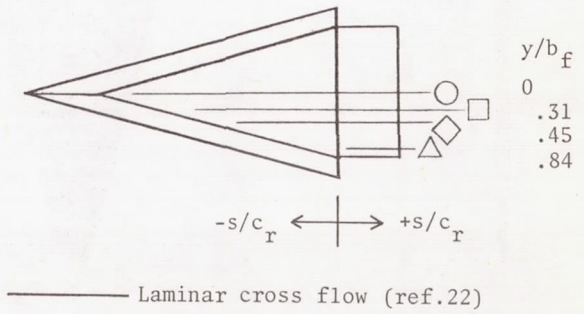

Figure 15.- Concluded.

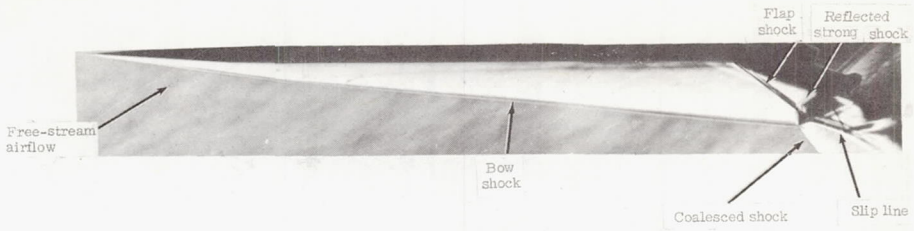

Schlieren photograph

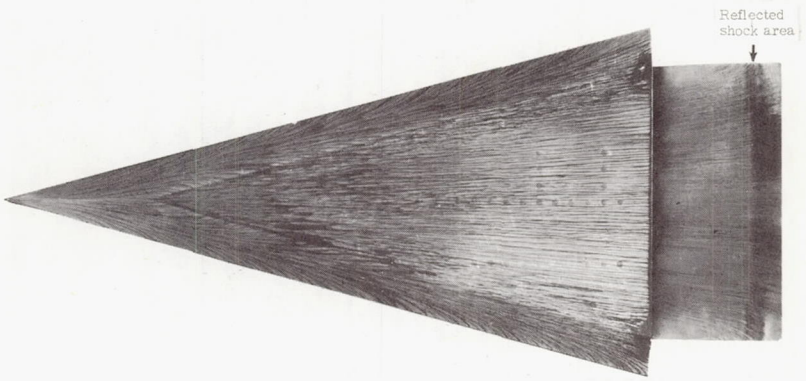

Oil-flow photograph

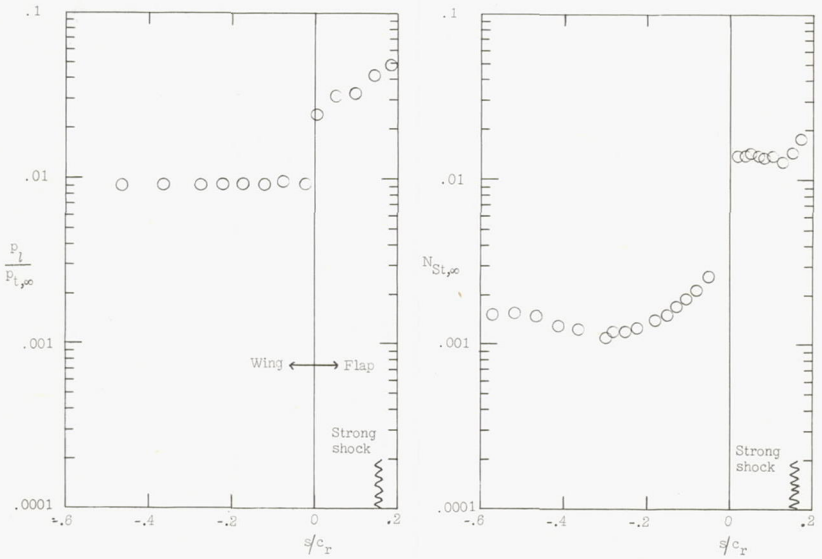

Center-line pressures and heat transfer

(a) $\alpha = 30^0$; attached flow. L-69-5249

Figure 16.- Details of bow-shock flap-shock interaction. $\delta = 20^0$; $R_\infty \approx 3.4 \times 10^6$.

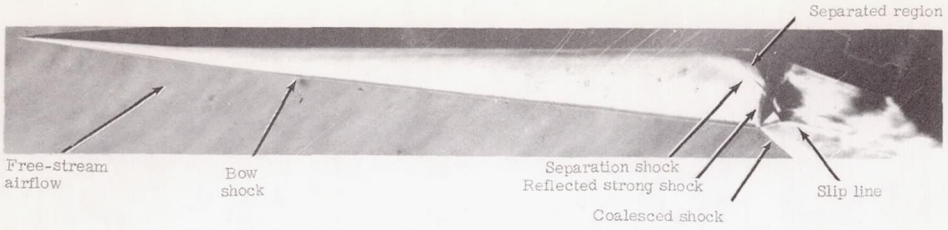

Schlieren photograph

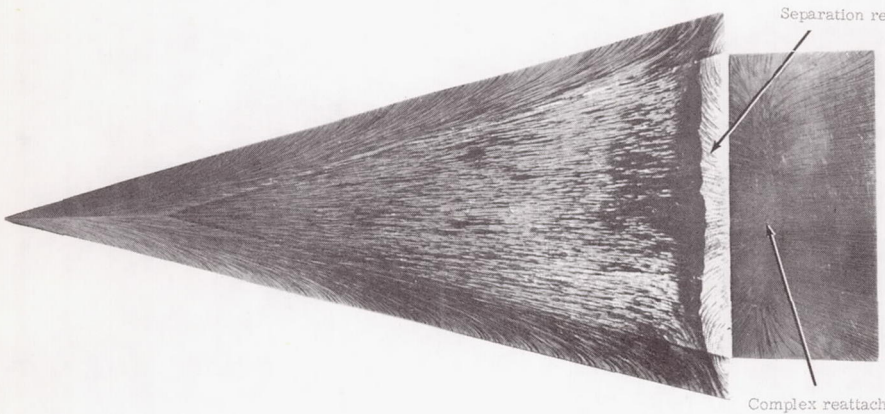

Oil-flow photograph

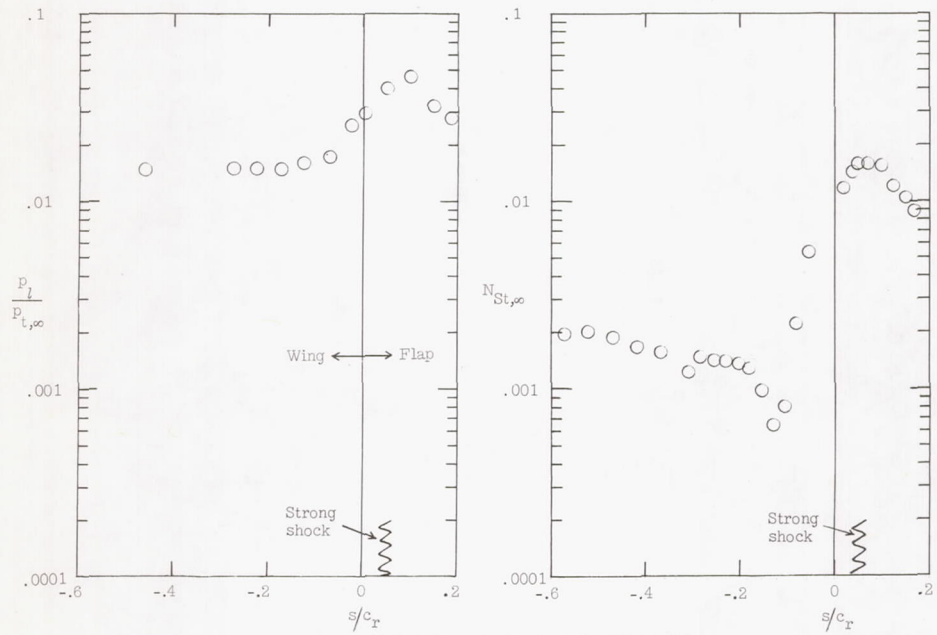

Center-line pressures and heat transfer

(b) $\alpha = 40^0$; separated flow.

Figure 16.- Concluded.

L-69-5250

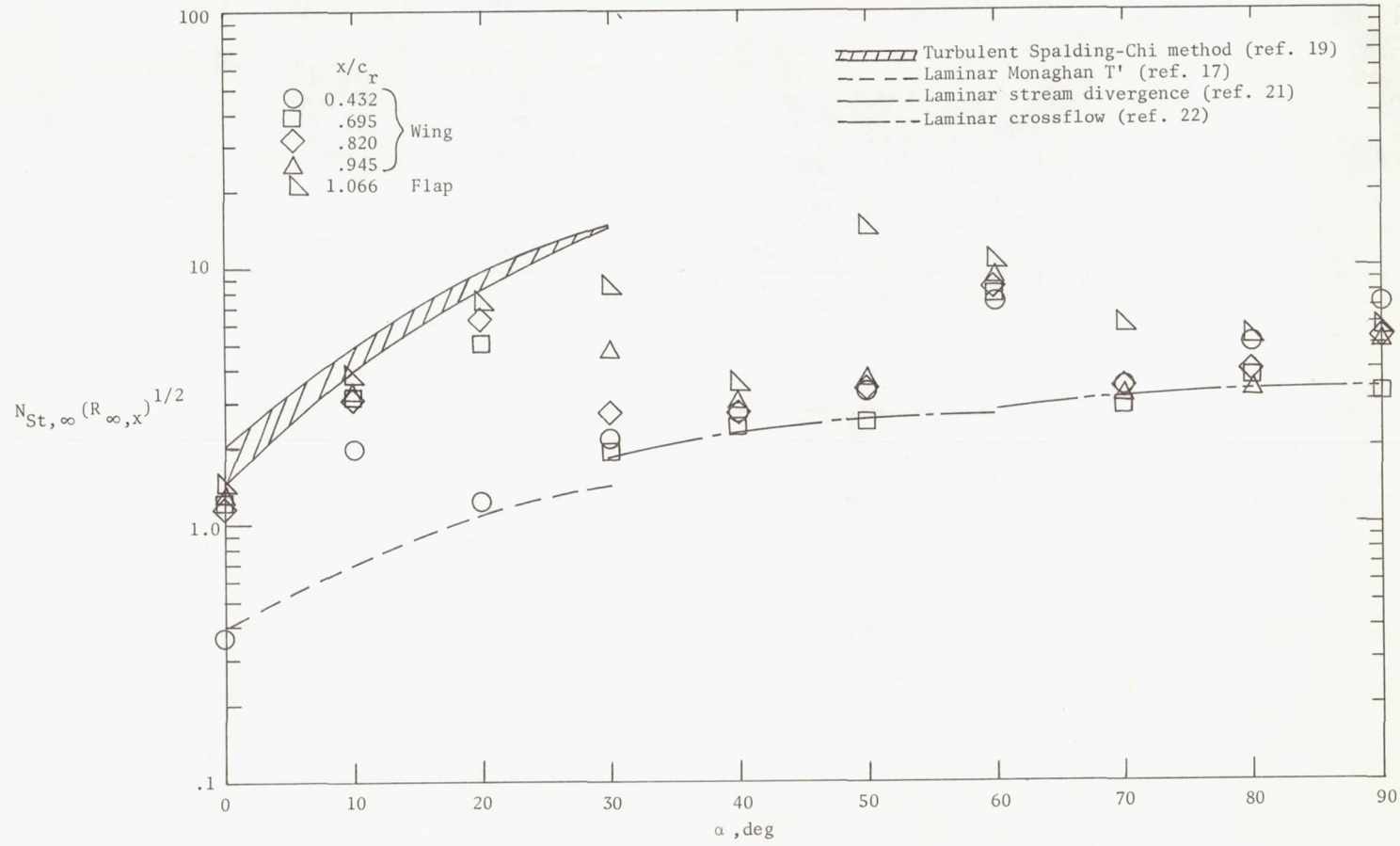

Figure 17.- Comparison of center-line heating with theory for the delta wing and flap over the complete angle-of-attack range. $\delta = 0^{o}$; $R_{\infty} \approx 3.4 \times 10^{6}$.